SOME MOLECULAR-BEAM MEASUREMENTS WITH A PIRANI DETECTOR

by

DANIEL LEWIS JASSBY

B.Sc., McGill University, 1962

A THESIS SUBMITTED IN PARTIAL FULFILMENT OF THE REQUIREMENTS FOR THE DEGREE OF

MASTER OF SCIENCE

in the Department

of

PHYSICS

We accept this thesis as conforming to the required standard

THE UNIVERSITY OF BRITISH COLUMBIA

September, 1964

In presenting this thesis in partial fulfilment of the requirements for an advanced degree at the University of British Columbia, I agree that the Library shall make it freely available for reference and study. I further agree that permission for extensive copying of this thesis for scholarly purposes may be granted by the Head of my Department or by his representatives. It is understood that copying or publication of this thesis for financial gain shall not be allowed without my written permission.

Department of Physics

The University of British Columbia,
Vancouver 8, Canada

Date October 15, 1964

ABSTRACT

A differential Pirani molecular-beam detector was developed with a sensitivity for noncondensable gases about five times greater than that of the previous most sensitive Pirani beam-detector. With a circular entrance channel of pressure-accumulation factor 28, at room temperature a one-microvolt signal was produced for a helium beam intensity of 5.4×10^{12} atoms/sec/cm^2. At liquid-nitrogen temperature, the sensitivity increased almost four times.

This detector was used to investigate the directivity characteristics of molecular beams of helium, argon and nitrogen, produced with several circular, cylindrical tubes, mounted on a rotatable oven. In the molecular-flow region, the angular distributions were somewhat narrower than those reported by previous workers. With increasing source pressure, the full-width at half-maximum of the distribution for each tube with any gas became 75 to 78 degrees, but with further increase of source pressure, the full-width depended on the particular gas used.

The electric circuit of the Pirani detector was easily modified so that the entrance channel and beam cavity could be used as a combination Pitot tube and pressure gauge for determining the Mach numbers of supersonic beams in vacuum. It was found that a 0.214-mm. conical converging nozzle

produced a Mach 2.2 helium beam when the pressure ratio across the nozzle was about 120.

ACKNOWLEDGEMENTS

The author wishes to thank Dr. J.B. Warren for his supervision of the work described in this thesis.

The author is grateful to Mr. D. Axen for his keen interest and generous assistance in the experimental work. Useful discussions with Dr. K.L. Erdman and Mr. C.W. Vermette are greatly appreciated. Thanks are due to Messrs. A. Fraser, P. Haas, and G. Lang for technical assistance.

The author would like to thank Dr. B.L. White and Dr. G. Jones for their invaluable guidance in the development of the ionization gauge control unit.

The author is indebted to the National Research Council of Canada for the two scholarships held during the course of this work.

TABLE OF CONTENTS

		Page
Chapter I	INTRODUCTION	1
Chapter II	DEVELOPMENT OF THE DIFFERENTIAL PIRANI DETECTOR	3
A.	Requirements for the Molecular-Beam Detector	3
B.	Types of Molecular-Beam Detectors	3
C.	Design of the Differential Pirani Detector	8
(1)	Principle of Operation	8
(2)	Theoretical Sensitivity for Helium-3	9
(3)	Construction	12
D.	Control of the Differential Pirani Detector	13
(1)	Mechanical Controls	13
(2)	Electric Circuit	14
Chapter III	TESTING OF THE DIFFERENTIAL PIRANI DETECTOR	16
A.	Experimental Arrangement	16
(1)	Vacuum System	16
(2)	Beam Source	17
B.	Operation of the Differential Pirani Detector	18
(1)	Stability	18
(2)	Verification of $1/r^2$ Detection	20
(3)	Calibration	22
(4)	Sensitivity for Helium-3	24
(5)	Conclusions	25

		Page
Chapter IV	DIRECTIVITY OF MOLECULAR BEAMS FROM CIRCULAR CYLINDRICAL TUBES	27
A.	Previous Measurements	27
B.	Apparatus	28
C.	Directivity Measurements	30
(1)	Experimental Procedure	30
(2)	Results	32
(3)	Conclusions	34
Chapter V	MACH NUMBERS OF MOLECULAR BEAMS PRODUCED WITH A CONVERGING NOZZLE	36
A.	Construction of Nozzles	36
B.	Measurement of Flow Rate	37
C.	Measurement of the Mach Number	39
(1)	Interpretation of Impact-Pressure Measurements	39
(2)	Modification of the Differential Pirani Detector	40
(3)	Impact-Pressure Measurements on Beams from the 0.214-mm Converging Nozzle	40
Chapter VI	SOME FURTHER ASPECTS OF BEAMS PRODUCED WITH THE CONVERGING NOZZLE	43
A.	Nature of the Measurements	43
B.	Experimental Procedure	46
C.	Results	47
D.	Conclusions	48

Page

APPENDIX A THEORETICAL ANALYSIS OF THE DIFFERENTIAL PIRANI DETECTOR 49

1. Equilibrium Pressure and Time Constant 49

2. Dependence of the Filament Temperature on Changes in Cavity Pressure 51

3. The Detector Output Signal as a Function of Pressure 53

APPENDIX B TRANSISTORIZED IONIZATION GAUGE CONTROL CIRCUIT 56

1. Introduction 56

2. Operation of the Hot-Cathode Ionization Gauge 56

3. General Description of the New Control Circuit 57

4. Detailed Description of the New Control Circuit 58

5. Deficiencies of the Circuit 61

APPENDIX C MEASUREMENT OF FLOW RATE THROUGH NOZZLES 62

BIBLIOGRAPHY 64

LIST OF TABLES

		Page
1	Zero Drift of the Pirani Detector	18
2	Inverse Sensitivities of the Pirani Detector with $\mathcal{K}$ = 28	24
3	Experimental and Theoretical Sensitivities of the Pirani Detector	25
4	Inverse Sensitivities for H_2 of Pirani Detectors with $\mathcal{K}$ = 1.	26
5	Dimensions of Circular Tubes	31

LIST OF FIGURES

Figure		Following Page
1	Schematic Diagram of the Differential Pirani Detector Block	8
2	The Pirani Detector Filaments Connected in a Wheatstone Bridge	8
3	The Differential Pirani Detector Block	12
4	Schematic Diagram of the Mechanical Controls of the Pirani Detector	13
5	Circuit Diagram for the Differential Pirani Detector	14
6	Schematic Diagram of the Vacuum System	16
7	Schematic Diagram of the Molecular-Beam Chamber, with some Components	16
8	Response of the Pirani Detector to Changes in the Residual Gas Pressure	19
9	Experimental Arrangement for Measuring Angular Distributions of Molecular Beams	28
10	Schematic Diagram of the Rotatable Beam-Source	29
11	Angular Distribution of a Nitrogen Beam from the 2-mm Aperture	30
12	Measured F.W.H.M. of the Angular Distributions of Molecular Beams from Circular Cylindrical Tubes	32
13	Angular Distributions of Molecular Beams from Circular Cylindrical Tubes in the Molecular-Flow Region	33
14	Conical Converging Nozzle and Holder	36
15	Flow of Helium-4 through some Conical Converging Nozzles at $20^{o}C$	38

Figure		Following Page
16	Stagnation-Pressure Rise in Pitot Tube vs Mach Number of Gas Flow	40
17	Circuit Diagram for the Pirani Gauge	40
18	Calibration Curve for Pitot-Tube Pirani Gauge, for Helium-4	40
19	Pitot-Tube Measurements of Mach Numbers of Helium-4 Beams from the 0.214-mm Conical Converging Nozzle	41
20	Geometry of the System for Probing Nozzle Beams	45
21	Effect of the Residual Gas Pressure on the Spatial Distribution of the Directional Kinetic Energy of a Nozzle Beam	47
22	Effect of the Source and Residual Gas Pressures on the Spatial Distribution of the Directed Kinetic Energy of Nozzle Beams	47
23	Spatial Distributions of the Directed Kinetic Energy of Two Nozzle Beams	47
24	Schematic Diagram of the Bayard-Alpert Ionization Gauge	56
25	Transistorized Ionization Gauge Control Circuit	58
26	Apparatus for Measuring Rate of Gas Flow through Nozzles	62

CHAPTER I

INTRODUCTION

In 1962 it was decided to attempt to construct in this laboratory an apparatus for producing a high intensity beam of nuclear-polarized, singly-charged, helium-3 ions. The scheme (Axen, Klinger and Warren, 1963) consists in essence of the following: An atomic beam source, maintained at 2.2°K, produces a supersonic helium-3 beam with a narrow velocity distribution centered at 180 m/sec. The beam then passes through a hexapole magnet which separates the atoms according to their nuclear spin states. The polarized atomic beam thus obtained enters an electron-bombardment ionizer (Vermette, 1964), and a nuclear-polarized ion beam is extracted from the side.

To measure the intensity of the atomic beam at various stages in the apparatus, some form of neutral beam detector is necessary. It was decided to construct a new version of the differential Pirani detector. A large high-speed vacuum system was built for testing the beam detector and the electron-bombardment ionizer.

The Pirani detector proved to be excellent in its performance. It was used to measure some directivity characteristics of helium, argon, and nitrogen molecular beams produced with a few circular, cylindrical tubes. This was done to verify

the results of Naumov, 1963, who had recently carried out with ammonia the first extensive investigation of the directivity of neutral beams produced with circular, cylindrical tubes.

The main component of the atomic beam source in the polarized - helium-3 apparatus is a 0.2-mm nozzle which must produce the supersonic beam. The construction of the Pirani detector was such that it could be used as a combination Pitot tube and pressure gauge to determine the Mach numbers of molecular beams produced with miniature nozzles, so that a suitable one could be chosen for the polarized - helium-3 apparatus.

CHAPTER II

DEVELOPMENT OF DIFFERENTIAL PIRANI DETECTOR

A. Requirements for the Molecular-Beam Detector

The nuclear-polarized He^3 beam emerging from the hexapole magnet is expected to have an intensity of about 3×10^{15} atoms/sec/cm^2; the intensity will be considerably less at the end of the ionizer. For ease in locating the beam and measuring the beam profile, it is desirable to have a metrical detector with a sensitivity of at least 10^{13} atoms/sec/cm^2 and a signal-to-noise ratio of at least 2:1 at this intensity. Linear response to beam intensity over a considerable range is advantageous.

For rapid determination of the beam position, the detector should have an equilibrium time less than 5 seconds and must be readily movable in vacuum. It is preferable that the detector be easy to construct, operate and repair.

B. Types of Molecular-Beam Detectors

Detectors have been discussed in considerable detail by Smith, 1955, King and Zacharias, 1956, Ramsey, 1956, and others. The most important types are examined below.

(1) In the Condensation Method, the beam condenses on a cooled glass surface, forming a deposit similar in shape to the beam profile. He^3, of course, is noncondensable

at easily obtained temperatures.

(2) Chemically-active molecules can be detected by a target which is visibly changed by chemical combination with the beam molecules. He^3, however, is probably chemically inert.

(3) In the Surface Ionization Detector, the beam molecules impinge on a hot surface and reevaporate. If the work function of the surface is greater than the ionization potential of the beam molecules, positive ions are formed and easily detected. However, no suitable material has a work function greater than 6 ev, which is much less than the ionization potential of He^3 (24.5 ev).

(4) The Radioactivity Method detects beams of radioactive isotopes by the radioactivity of their deposits on a condensation target. He^3 is not radioactive.

(5) The Electron-Bombardment Ionizer ionizes a fraction of the beam which is then extracted, analyzed with a mass spectrometer, and measured with a suitable ion current amplifier. For good resolution, a directional entrance on the ionizer is necessary; then the number of background atoms in the ionizer may be several orders-of-magnitude larger than the number of beam atoms, so that modulation of the beam is essential. This method would probably have adequate sensi-

tivity and signal-to-noise ratio; however, it is quite complicated to construct and there might be difficulty in moving the whole assembly in vacuum.

(6) The Differential Ionization-Gauge and (7) The Differential Pirani-Gauge Detectors are differential manometers which measure pressure inside small receiving vessels. The ionization detector consists of two identical ionization gauges, each completely closed except for an entrance channel, while the Pirani detector consists similarly of two identical Pirani gauges, which are usually enclosed in one metal block. With either detector the beam is directed into one of the gauges, raising the pressure inside by an amount proportional to the beam intensity. This pressure increase can be multiplied by a large factor (the kappa factor K) by using a low-conductance channel for the gauge entrance; the beam travels down the channel without hitting the sides, while molecules inside the gauge can emerge only after many collisions, on the average, with the channel walls. The second gauge of each detector is used to balance out fluctuations in the residual gas pressure, P_v.

In Appendix A it is calculated that for a gauge with an aperture of negligible length to admit the beam ($K = 1$), a beam intensity of 10^{13} atoms/sec/cm^2 of He^3 produces a pressure increment in the gauge of 8.5×10^{-9} mm Hg at room temperature. Using extremely stable (0.002%) electron-

emission regulators, Hurlbut, 1958, has built a differential ionization-gauge detector with a sensitivity of 2×10^{-5} times P_v. Thus for $P_v = 10^{-5}$ mm Hg and a 2:1 signal-to-noise ratio, this detector has a sensitivity of 8×10^{-10} mm Hg; a He^3 beam of intensity 10^{13} atoms/sec/cm^2 would produce a signal $\sim$10 mV.

The most sensitive differential Pirani detector built before the present work produces a 1 microvolt signal for a H_2 pressure of 6×10^{-7} mm Hg, with noise and short-term drift below 1 microvolt (Ellett and Zabel, 1931). Thus with this detector an entrance channel with $K \sim 100$ would be necessary for the required sensitivity.

It is noteworthy that Pirani detectors have a linear range of response with the same calibration up to total pressures of at least 10^{-3} mm Hg, while ionization gauges tend to perform erratically and nonlinearly above 10^{-4} mm Hg.

The equilibrium times of the two detector types can be made comparable, since while the thermal time constant of moderately heated Pirani filaments is $\sim$1 second, the comparatively large volume of the ionization gauge is responsible for a similar time constant.

For operation, the Pirani detector requires a stabilized low-voltage power supply (a battery is often suitable) and an extremely sensitive galvanometer, while the ionization detector requires two extremely well-stabilized

electron-emission regulators and a sensitive ion current amplifier.

Thus the ionization detector has a limited upper range and requires more elaborate electronic equipment than the Pirani detector. However, it has the advantages of much higher sensitivity and greater signal output for a given incident beam intensity.

Nevertheless it was decided to build a Pirani detector because of the commercial availability of matched pairs of small tungsten filaments; viz., Gow-Mac* type W-2. These made the construction of a Pirani detector much easier than that of an ionization detector, and offered the possibility of achieving significantly greater sensitivity than previously possible with Pirani detectors. These filaments, developed for gas chromatography purposes, consist of a 12" length of 0.001" -diameter tungsten wire coiled in two helices and mounted on a small brass flange. Two filaments can be enclosed in a volume $\sim$1 cc, which is desirable for a small filling time constant. It was thus unnecessary to work with ribbon filaments with attendant problems of mounting difficulties, noise produced at the supports, and contact of the ribbons when heated with the gauge wall.

---

* Available from Gow-Mac Instrument Company, 100 Kings Road, Madison, New Jersey, U.S.A.

C. Design of the Differential Pirani Detector

(1) Principle of Operation

Differential Pirani molecular-beam detectors were first constructed and investigated thoroughly by Knauer and Stern, 1929, and Ellett and Zabel, 1931. The detector (figure 1) usually consists of four moderately heated filaments, R_{1-4}, in two identical cavities, C_1 and C_2, in a metal block, which are connected with the surrounding vacuum by identical channels K_1 and K_2. The two filaments in each cavity form the opposite arms of a Wheatstone bridge which is initially balanced (figure 2). The condition of balance is $R_1 \times R_2 = R_3 \times R_4$. R_1 and R_3 are filaments matched for both resistance and temperature coefficient of resistance; similarly for R_2 and R_4. Then fluctuations in the residual gas pressure in the vacuum system will have identical effects on the temperatures and thus resistances of R_1 and R_3, and of R_2 and R_4, so that the bridge remains balanced. The effect of ambient temperature and supply voltage fluctuations on the balance is also markedly reduced with matched filaments (Leck, 1957). In order for the balance to be effective, C_1 and K_1 must be identical to C_2 and K_2, respectively, so that the filling time constants of the two cavities are the same.

The detector block is positioned so that the longitudinal axis of K_1 is aligned parallel to the incident beam

FIGURE 1. Schematic Diagram of the Differential Pirani Detector Block. R_1, R_2, R_3 and R_4 are the Pirani filaments.

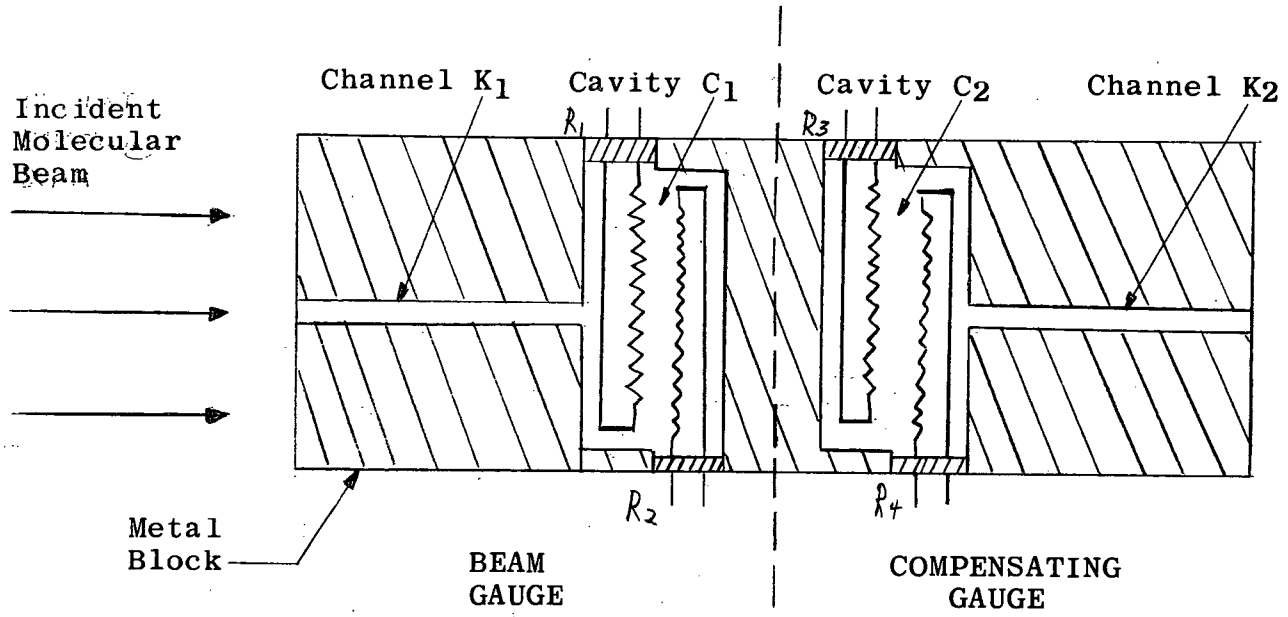

FIGURE 2. The Pirani Detector Filaments Connected in a Wheatstone Bridge.

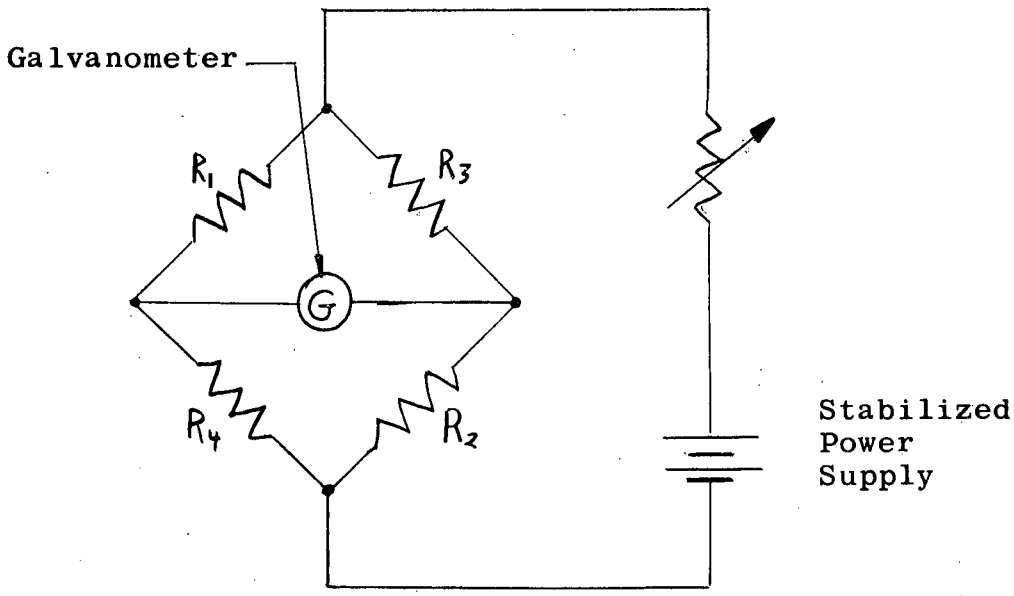

direction (Figure 1). Then as shown in Appendix A the pressure in C_1 increases above that in C_2 to an equilibrium value P_d given by

$$P_d = \mathcal{K} I \sqrt{2\pi m k T_d} \qquad \text{(Eq. 1)}$$

where $\mathcal{K}$ is the accumulation factor of K_1,

I is the incident beam intensity,

m is the mass of a beam molecule,

k is Boltzmann's molecular gas constant, and

T_d is the temperature of the detector block.

This pressure increment cools filaments R_1 and R_2 because of greater heat conduction by the gas from the filaments to the wall of C_1. Thus the resistances of R_1 and R_2 decrease, producing an out-of-balance signal on the bridge galvanometer.

(2) Theoretical Sensitivity for He^3

The theoretical sensitivity of the Pirani detector using the W-2 tungsten filaments is calculated in Appendix A. The results are presented here.

The electrical energy supplied to the filaments is dissipated by three processes: (a) Conduction through the end supports, which can be neglected, because the filaments are very long (6" helices) compared to their diameter (0.001"); (b) radiation to the cavity wall, which is independent of gas pressure; and (c) gas conduction from the filaments to the cavity wall, which depends on the gas pres-

sure in the cavity.

Suppose that the bridge galvanometer has extremely high resistance compared to the filament resistance and that the bridge is supplied with a constant-current source. If an incident molecular beam raises the pressure in C_1 by an amount dP_d, then as shown in Appendix A the corresponding galvanometer signal will be

$$dV = \frac{(T_f - T_d)}{(T_f)^3} \sqrt{(T_f^4 - T_d^4)R_f} \sqrt{\frac{S}{\sigma \epsilon}} \frac{(c\beta)}{4} dP_d \qquad \text{(Eq.2)}$$

where dP_d is found from Eq. 1,

$$\beta = \frac{C_v \alpha}{N_o} \frac{1}{\sqrt{2\pi m k T_d}} \qquad \text{(Eq. 3)}$$

C_v is the specific heat of the gas per mole at constant volume,

N_o is Avogadro"s number,

α is the thermal accomodation coefficient of the gas on the filament surface,

S is the surface area of one filament,

c is the temperature coefficient of resistance of the filament,

T_f is the filament temperature,

R_f is the filament resistance at T_f,

ϵ is the emissivity of the filament,

σ is the Stefan-Boltzmann radiation constant,

and the other quantities have been defined before.

Eq. 2 is valid provided the mean-free-path of the gas

molecules is much greater than any dimension of C_1. If the maximum cavity dimension is 1.5 cm, this restricts the total cavity pressure for helium to about 2 microns at $T_d = 293^oK$ and 0.5 micron at 77^oK. Since the changes in T_f with P_d are very small, below these pressures the sensitivity dV/dP_d is constant, so that the gauge has a linear response in this range.

Once the Pirani filaments are chosen, most of the parameters of Eqs. 2 and 3 are fixed. However, the sensitivity can be optimized by choosing a suitable bridge current and thus T_f. Eq. 2 shows that the sensitivity increases monotonically with T_f, the temperature-dependent factor approaching $1/\sqrt{R_f}$ when $T_f \gg T_d$. However, the safe upper limit for the W-2 filaments is $R_f = 92$ ohms, corresponding to $T_f = 560^oK$. With this operating temperature and with $K = 1$, it is shown in Appendix A that a He^3 beam of intensity 10^{13} atoms/sec/cm^2 will theoretically produce the following detector signals: 0.15 microvolt at $T_d = 293^oK$ and 0.28 microvolt at $T_d = 77^oK$.

In previous Pirani detectors noise and short-term drift could be reduced below $1\,\mu V$. If we assume it will be $1\,\mu V$ in the present detector, then at room temperature for a 2:1 signal-to-noise ratio at $I = 10^{13}$ atoms/sec/cm^2, K must be greater than 14.

In Appendix A it is shown that the time constant for filling and emptying a gauge cavity is

$$\tau = K \frac{V_d}{A_d} \sqrt{\frac{2\pi m}{kT_d}} \qquad \text{(Eq. 4)}$$

where V_d is the volume of the cavity,

A_d is the cross-sectional area of the entrance channel, and the other quantities have been defined before.

Thus K cannot be made indefinitely large because of the inconvenience of long equilibrium times. Moreover, the difficulty of aligning the detector is aggravated with increasing impedance of the entrance channel. The value actually chosen was $K = 28$.

(3) Construction

Figure 3 shows the actual detector block. The material used was brass to reduce thermal gradients and thus minimize zero drift (Ellett and Zabel, 1931).

Eq. 4 shows that for minimum τ, V_d must be made as small as possible. Two identical cavities were drilled in the brass block just large enough to enclose two W-2 filaments each; V_d was approximately 1.3 cc. Channels K_1 and K_2 each consisted of a $1\frac{1}{8}$" length of German silver tubing, with I.D. 0.80 mm and O.D. 1.0 mm, so that $K = 28$ (Dushman and Lafferty, 1962). 1.0-mm holes were drilled from the cavities to opposite sides of the block; the two channels were placed in these and sealed with soft solder. The flanges supporting the filaments were carefully centered on their mounting seats and sealed with soft solder.

SCALE 2:1

Four $\frac{17}{64}$" holes drilled 0.781" deep, then conterbored $\frac{3}{8}$" to $\frac{1}{32}$" depth.

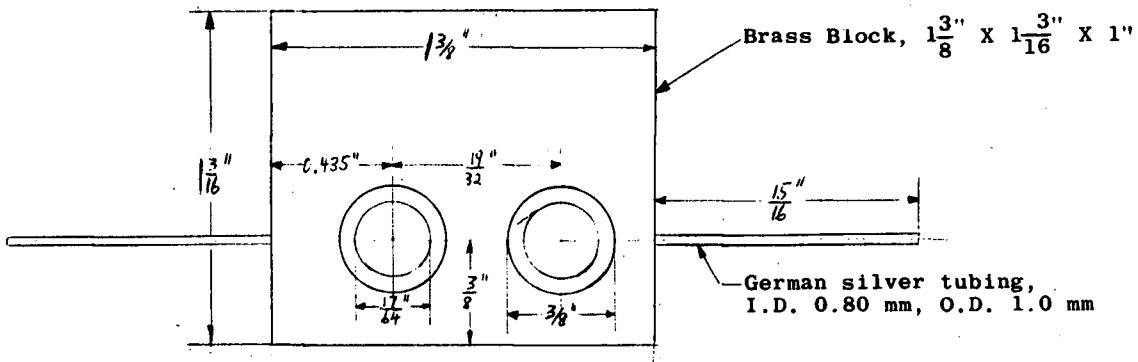

(a) Mounting positions of Pirani filaments R_1 and R_3.

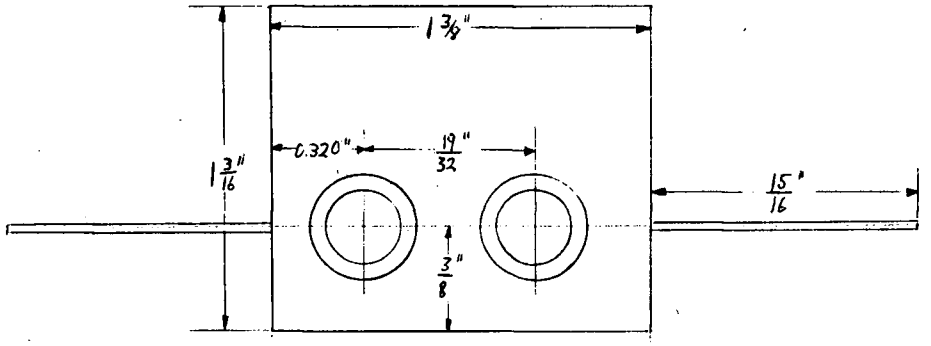

(b) Mounting positions of Pirani filaments R_2 and R_4.

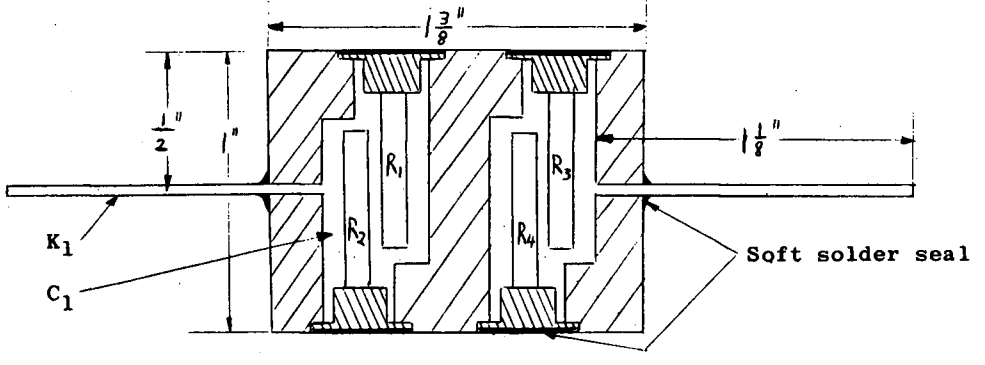

(c) Section through the filament axes. (Gow-Mac type W-2 filaments.)

FIGURE 3. The Differential Pirani Detector Block.

Using the above detector dimensions, from Eq. 4 it is calculated that γ = 0.20 sec at T_d = 293°K and 0.39 sec at T_d = 77°K. These times are smaller than the thermal time constant of the filaments (~1 sec).

D. Control of the Differential Pirani Detector

(1) Mechanical Controls

In the polarized-He^3 apparatus it will be convenient to install the detector from a vertical flange on the vacuum chamber. Thus the arrangement shown in Figure 4 was used to support the detector block. The block was silver-soldered to a 1/2" O.D. stainless steel tube (for minimum bending), the end of which could be joined by a short hose to another tube soldered to a styrofoam-insulated metal container holding liquid N_2. The detector could thus be maintained at 77°K, provided a 3/16" copper tube was inserted down the steel tube via the liquid-N_2 container in order to provide a means of escape for air upon filling as well as for evaporated N_2. The steel tube was insulated from supporting flanges by vacuum and a thin-walled outer steel tube.

The detector block could be moved horizontally up to 7 cm by compression of the bellows and about 1 cm from the central position in any direction in the vertical plane by shear motion of the bellows. The detector could also be tilted up to a few degrees in any direction by suitable

FIGURE 4. Schematic Diagram of the Mechanical Controls of the Pirani Detector. Flange A bolts on to a vertical port of the vacuum chamber.

Scale: ~1:2

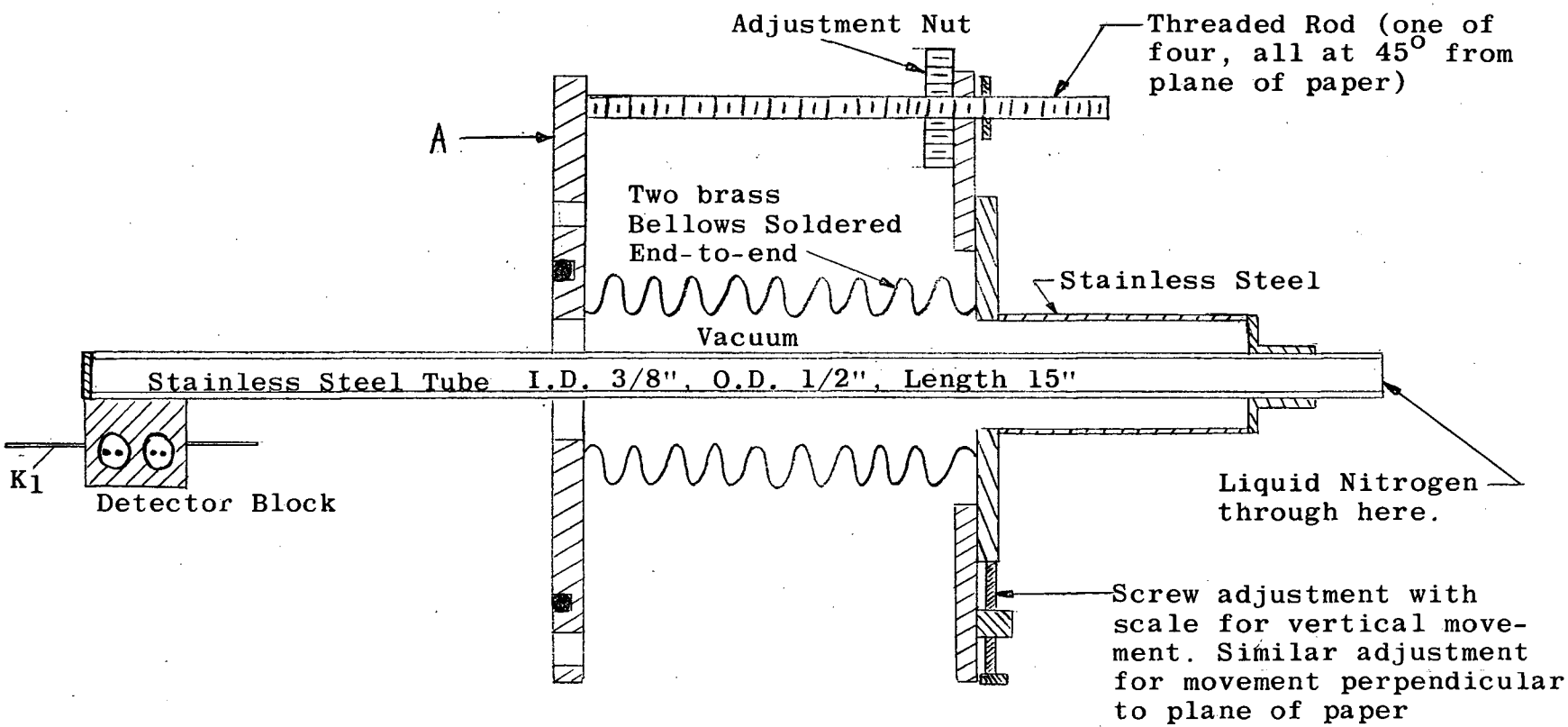

turning of four adjustment nuts. These means of adjusting detector position and orientation were invaluable for aligning channel K_1 with an incident molecular beam.

(2) Electric Circuit

The filaments were connected in the Wheatstone bridge circuit shown in Figure 5. A 0-10 V, 100 mA voltage supply stabilized to 0.1% was used to supply bridge current. For the null-point indicator, G, it was most convenient to use an electronic dc amplifier of high impedance. Two were available: Honeywell Model 1000Ω had a maximum sensitivity of about 0.5 μV/mm, with negligible noise and short-term drift; it was inconvenient, however, for quantitative measurements because no calibrated scales were provided, but merely a control for varying the sensitivity. Hewlett-Packard Model 425A with virtually infinite impedance was suitable for quantitative measurements. The most sensitive scale was 10 μV F.S.D. with negligible drift; however on all scales noise amounted to about 2 μV peak-to-peak.

A balancing network was provided for the bridge, since at any heating current the resistances of a filament pair were not exactly equal. The 1-ohm pot. was used for rough balance, with finer balancing obtained by adjustment of the 10- and 100-ohm pots.

Two 10 W- 100-ohm flat-sided power resistors were fastened securely to the detector block, so that when 30 V

FIGURE 5. Circuit Diagram for the Differential Pirani Detector.

R_1, R_2, R_3 and R_4 are the Pirani filaments (Gow-Mac Type W-2.)

Resistances in ohms. All resistors 10%, 1/2 W, unless otherwise noted.

All potentiometers wirewound, 5 W.

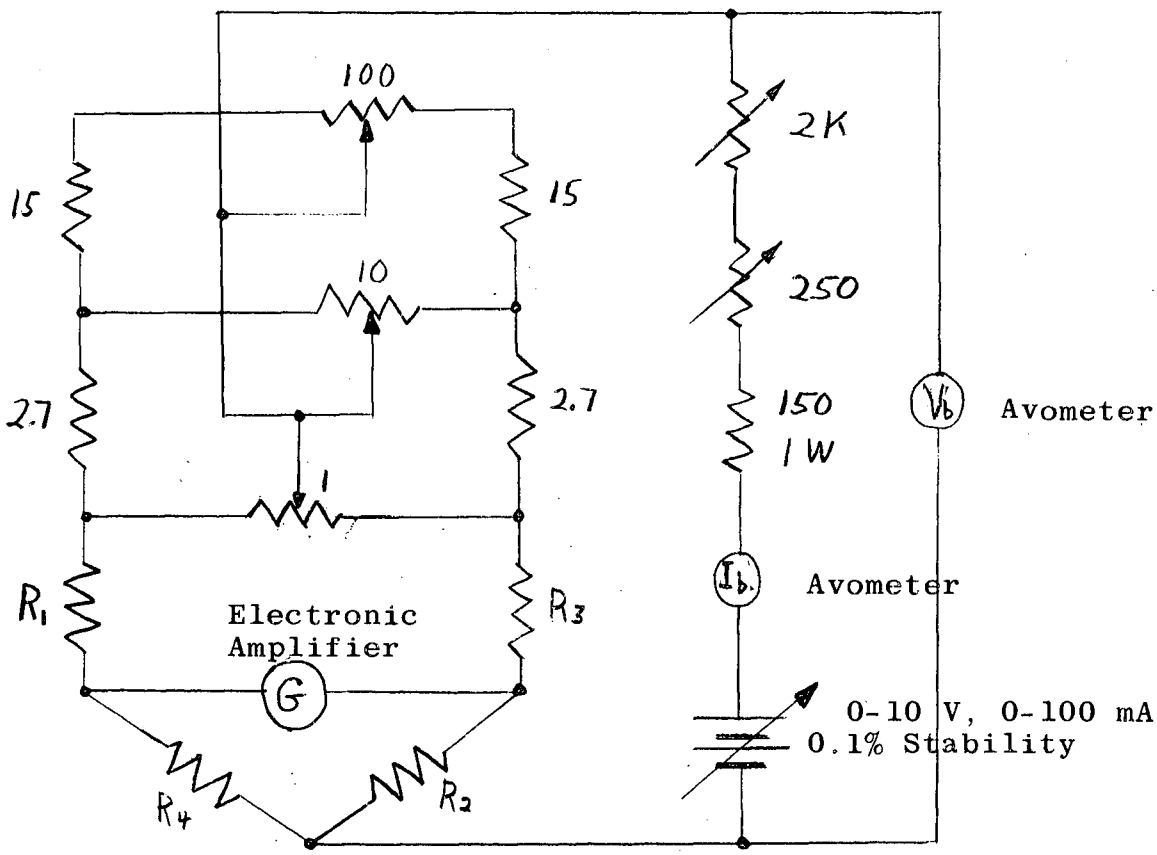

was applied to them under high vacuum, the block temperature was raised to 130°C in about one hour; this was a useful means of outgassing the detector cavities. A copper-constantan thermocouple attached to the block indicated its temperature.

Formel magnet wire was used in the vacuum system for electrical connection to the filaments and heating resistors. These leads and those of the thermocouple were connected with the external circuitry by means of glass-to-metal seals on a nearby flange of the vacuum chamber (Figure 7).

CHAPTER III

TESTING OF THE DIFFERENTIAL PIRANI DETECTOR

A. Experimental Arrangement

(1) Vacuum System

A 23-liter brass vacuum chamber was designed for testing molecular-beam sources, detectors and ionizers (Figure 7). Large pumping speeds are necessary for working with molecular beams. There were available two D.P.I. MCF-700 oil diffusion pumps with a cold-trap and plate-valve manifold fabricated of mild steel. This manifold was somewhat modified and joined together with the water-cooled baffled pumps and beam chamber as shown in Figure 6.

Low vacuum was measured with inexpensive thermocouple gauges, while high vacuum ($\lesssim 10^{-3}$ mm Hg) was measured with an ionization gauge at the end of a high-conductance arm of the manifold. The ion gauge was operated with a newly-designed control circuit, described in Appendix B.

Pumping speeds for air and He^4 in the beam chamber were measured by the mercury-pellet method (Yarwood, 1956). In the range 2×10^{-6} to 2×10^{-4} mm Hg, the speed for air was 300-350 liters/sec and that for He^4 was about 400 liters/sec. The flatness of the speed curves in this range is expected for well-baffled pumps. The ultimate pressure of the system was about 5×10^{-7} mm Hg with liquid N_2, and about

FIGURE 6. Schematic Diagram of the Vacuum System

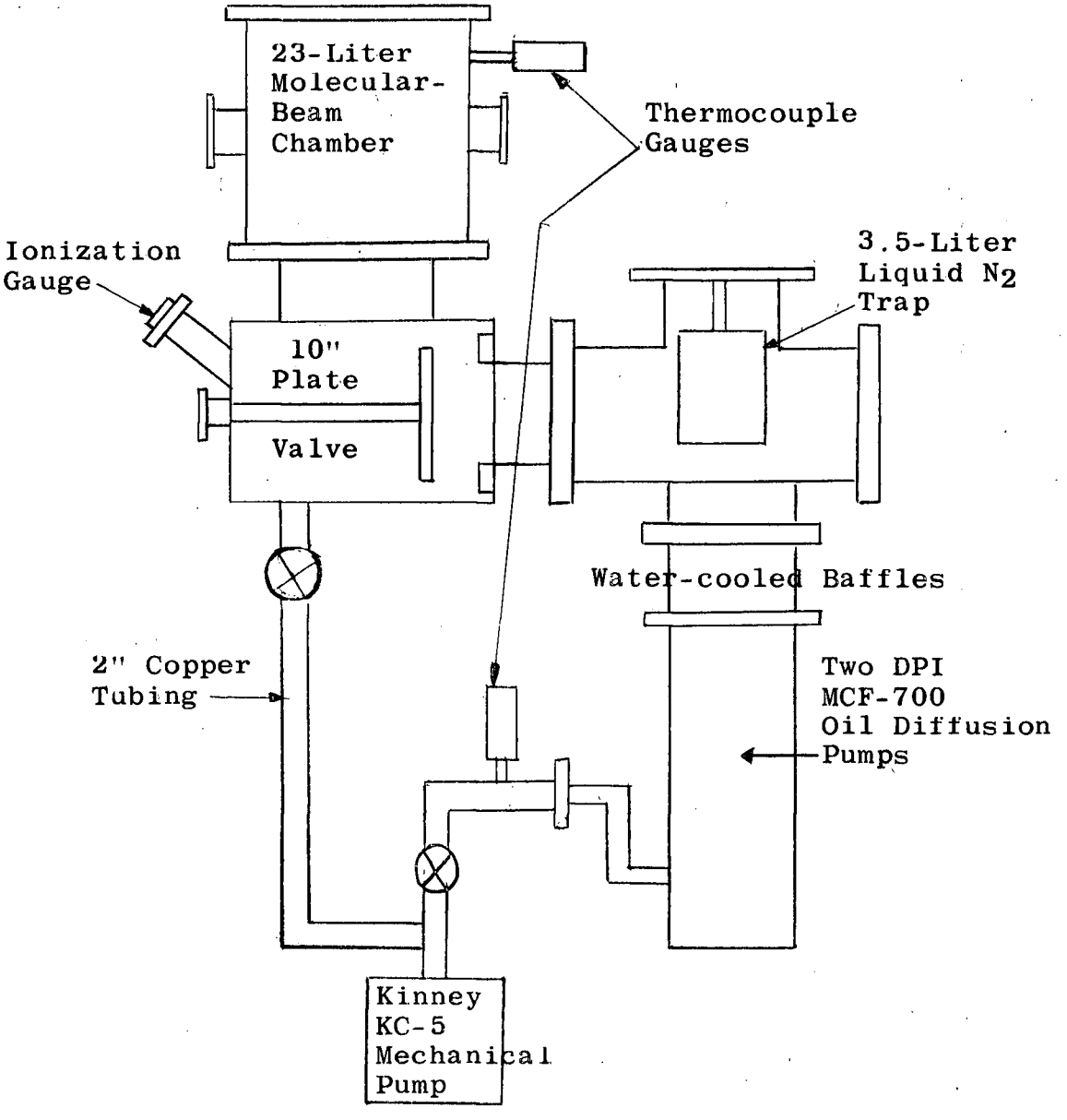

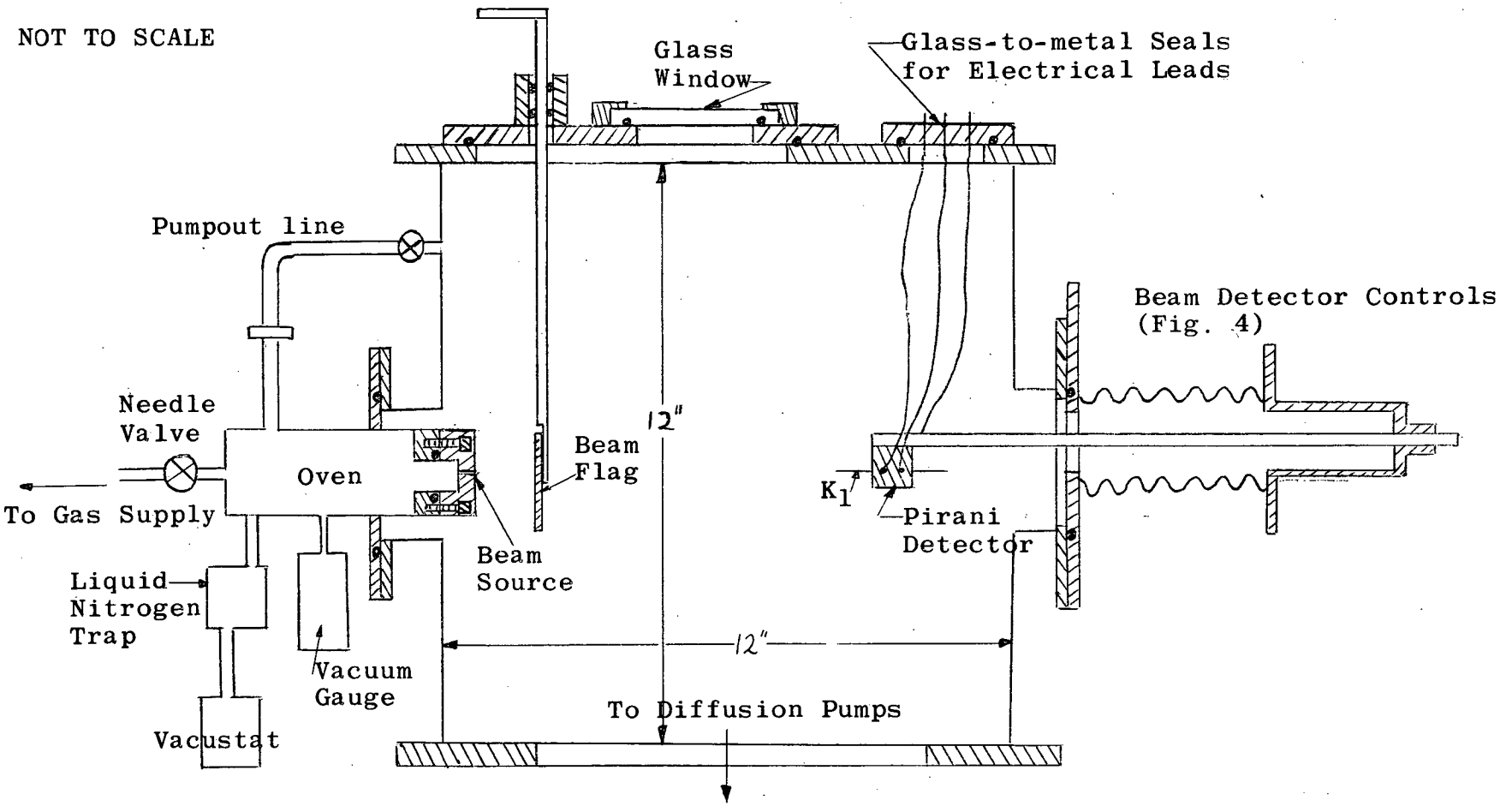

FIGURE 7. Schematic Diagram of the Molecular-Beam Chamber, with some Components.

1×10^{-5} mm Hg without.

(2) Beam Source

A molecular-beam source consists of a vessel, generally called an "oven", filled with a gas or vapor and equipped with an aperture, canal, or nozzle for the effusion of the molecules. In the present case the oven was a small brass chamber (Figure 7) to which could be bolted small flanges containing suitable canals or supporting nozzles. The gas flow to the oven was controlled with a fine needle valve. The oven could be evacuated by opening a valve connecting it with the beam chamber.

The following vacuum gauges were used to measure oven pressure: (a) a thermocouple gauge for rough measurement of pressure between 1 and 1000 microns; (b) a sensitive Pirani gauge (Edwards #M5B-2) for 10% accuracy between 0.1 and 60 microns, if zeroed before use; (c) a miniature McLeod gauge (Edwards vacustat, Model 2E) equipped with a cold trap, for 10% accuracy between 5 and 1000 microns; and (d) a mercury manometer for pressures in excess of 1 mm Hg.

The beam could be interrupted with a beam flag of copper sheet actuated by means of an O-ring-sealed shaft. This made it possible to observe any drift of the beam detector without closing the needle valve.

B. Operation of the Differential Pirani Detector

(1) Stability

To insure reasonable stability, the detector cavities had to be outgassed by pumping under high vacuum for many hours, although this time could be appreciably shortened by heating the gauge block at 150°C for 2 hr by means of the power resistors.

The following stability measurements were made after the detector had been pumped under vacuum better than 2 X 10^{-6} mm Hg for 24 hr. The galvanometer used was the Honeywell null indicator on its most sensitive setting (about 0.5 μV/mm). In Table 1, I_b and V_b are the bridge current and voltage respectively. The filament temperature T_f was calculated from $V_b/I_b = 40\left[1 + 0.005(T_f - 298)\right]$ (Eq. 5)
D_o is the peak-to-peak drift of the detector zero over a 30-minute period. The detector block was at room temperature and the vacuum better than 2 X 10^{-6} mm Hg.

TABLE 1

ZERO DRIFT OF PIRANI DETECTOR

I_b - mA	V_b - V	T_f - °K	D_o - μV
5.0	0.19	290	1
10.0	0.42	310	2
20.0	1.04	360	2
30.0	1.87	410	5
40.0	3.0	475	-

At I_b = 40.0 mA it was impossible to balance the bridge.

The pressure P_v in the beam chamber was then raised by admitting helium via a needle valve in a side port, and the off-balance deflection D_o observed at various I_b and P_v up to the maximum likely to occur in practice (Figure 8).

The above results show that the stability decreases with increasing T_f. However, the theory indicates that the greater T_f the greater the detector sensitivity (page 11). Thus in practice it was necessary to choose a T_f which gave good stability with as high a sensitivity as possible. The stability at I_b = 30.0 mA was inadequate while that at 20.0 mA was essentially the same as that at 10.0 mA. Hence it was decided to operate the detector at I_b = 20.0 mA ($T_f = 360^oK$).

By sending tap water down the stainless steel tube at various flow rates, it was observed that a large part of the instability was due to changes in block temperature. Even at fairly constant flow rate the zero drift was much greater then the drift when the block was subject to only room temperature variations.

When the detector temperature was reduced to 77^oK, a stable zero was obtained almost immediately with $I_b \leq 25.0$ mA, since outgassing was almost eliminated and the block temperature could not drift.

At room temperature with I_b = 20.0 mA, a 1% change in

FIGURE 8. Response of the Pirani Detector to Changes in the Residual Gas Pressure.

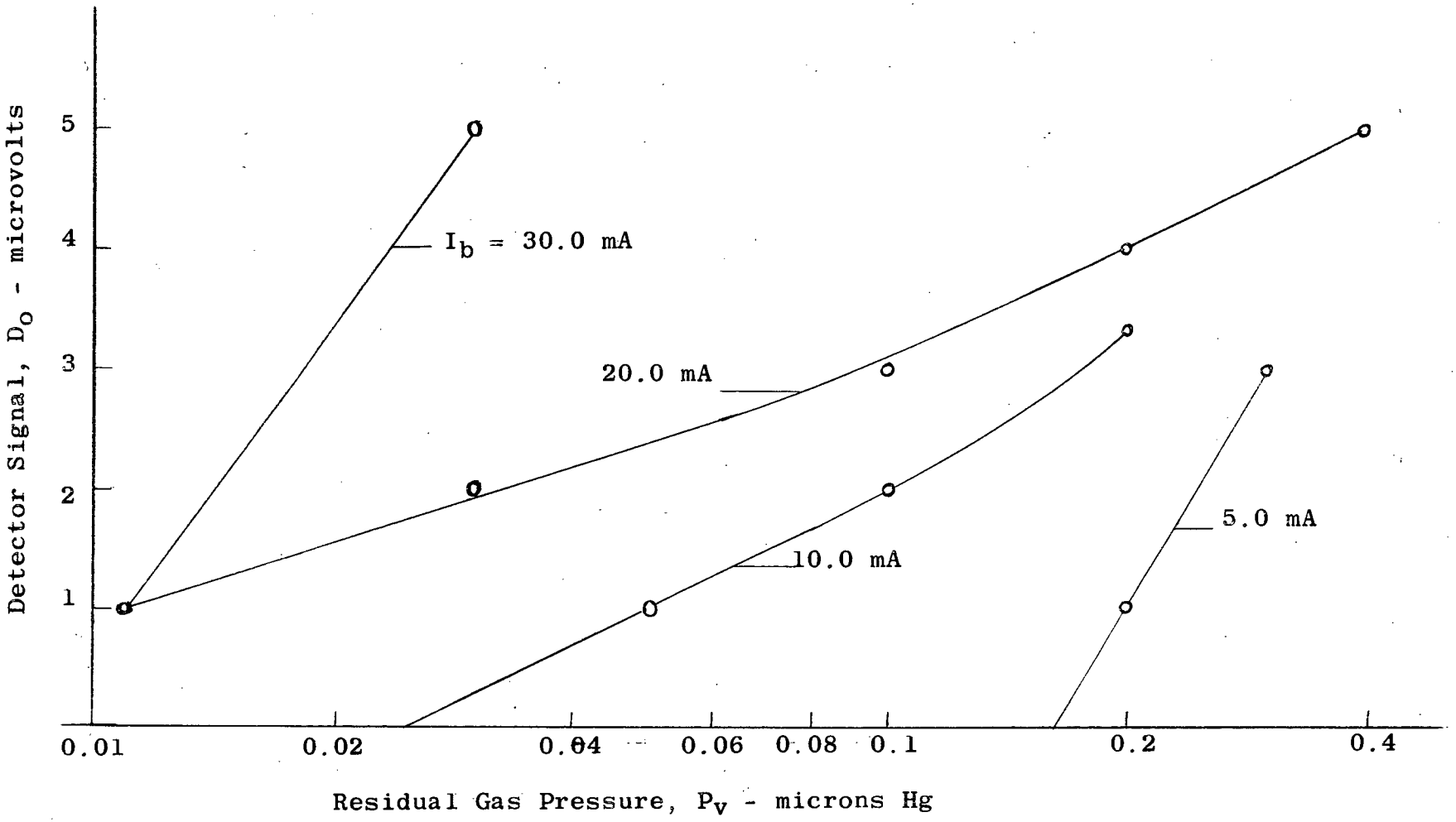

I_b caused an off-balance deflection of $\sim 20\,\mu V$, so the bridge power supply had to be current-stabilized to 0.1% or better.

The detector noise was negligible when the block was stationary. However, moving the block sometimes caused rather sudden off-balance signals as large as tens of microvolts. This was discovered to be mainly due to the detector leads in the vacuum chamber vibrating and knocking each other. It is also possible that sudden movement of the detector caused the filaments to vibrate and produce noise. This noise could be almost eliminated by using a suitable combination of rigid and flexible wire so that there was no contact between detector leads, and by moving the block slowly.

(2) Verification of $1/r^2$ Detection

To determine whether the Pirani detector could reliably detect a molecular beam, a helium beam was produced and the detector output D observed as a function of the source-detector distance, r. The relation between D and r should be $D \propto 1/r^2$ provided that the mean-free-path λ of the beam molecules in the beam chamber is such that $\lambda >> r$.

The beam source was a canal with length and diameter 0.79 mm, drilled in a brass flange bolted to the oven (Figure 7). With the whole system at atmospheric pressure, a light probe was inserted through the vacuum connection in the back of the oven; at r = 16 cm the detector orientation

was adjusted until the light beam emerging from the source appeared to hit squarely the entrance channel K_1, as observed from side and top ports of the beam chamber. The beam chamber was then pumped to $P_v \sim 1.5 \times 10^{-6}$ mm Hg, the detector was outgassed, and I_b set at 20.0 mA.

A source pressure of 65 microns of helium produced an outflow of gas through the canal which raised P_v to about 1.5×10^{-5} mm Hg. Thus $\lambda \sim 10$ meters. The range of r was $143 \leq r \leq 201$ mm, so that $\lambda >> r$.

At increments of r of about 10 mm, the detector was aligned precisely with the beam by carefully turning the adjustment nuts (Figure 4) until maximum deflection of the galvanometer was obtained. Before each reading the beam flag was lowered to observe any drift in the detector zero.

It appeared that the detector equilibrium time was about 4 sec, so that the time constant was about 1 sec. This was the thermal time constant of the filaments, since the filling time constant $\tau = 0.20$ sec, and the galvanometer time constant was negligible.

If $D \propto 1/r^2$, Dr^2 should be constant. At each r the measured value of Dr^2 was within 5% of the mean. The small deviations were probably mainly due to imperfect alignment of the detector.

Thus the detector appeared to give authentic detection of a molecular beam.

(3) Calibration

The detector was calibrated with a beam source consisting of a 2.0-mm aperture, made by piercing a 2.0-mm hole in 0.001" brass shim stock soft-soldered over a 5/16" hole in a brass flange, which was bolted to the oven (Figure 7). The beam intensity from an "infinitely-thin" aperture of this type is

$$I(\theta) = 1.11 \times 10^{22} \frac{A_S P_S}{r^2 \sqrt{M T_S}} \cos\theta \qquad \text{(Eq. 6)}$$

where $I(\theta)$ = beam intensity in molecules/sec/cm^2 at distance r cm from the aperture, and θ is the angle between the aperture axis and the line joining the point of observation to the aperture,

P_S = pressure of the gas in the oven, in mm Hg,

T_S = oven temperature, in ^oK,

A_S = area of the aperture, in cm^2, and

M = molecular weight of the gas, in gm.

In practice Eq. 6 is valid when the mean-free-path of the gas in the oven is at least as large as the diameter of the circular aperture (Ramsey, 1956).

If $\theta < 8^o$, $I(\theta) \geq 0.99\ I(0)$, according to Eq. 6. Thus for r = 182 mm, the point of observation in this case, the detector entrance could be displaced from the aperture axis by as much as 25 mm, with less than 1% error in the calculation of beam intensity. In any event channel K_1 had to point directly at the aperture; this was achieved by carefully

adjusting the detector orientation to obtain maximum galvanometer deflection.

The detector was calibrated for H_2, He^4, N_2 and Ar with I_b = 20.0 mA and T_d = 293°K. P_s was measured with the Edwards Pirani gauge which had been calibrated with a McLeod gauge and zeroed immediately before use. The detector was aligned with the aperture beam at r = 182 mm. With each gas the detector signal, D, was measured for increasing P_s up to the point where $P_v \sim 5 \times 10^{-5}$ mm Hg. Each value of D was corrected for scattering in the beam chamber; this amounted to as much as 17% (for Ar at 5×10^{-5} mm Hg: exp(-182/1000) = 0.83). The sensitivities of the ion gauge for these gases were taken from Dushman and Lafferty, 1962.

The corrected values of D were plotted against P_s and the slope $\nabla D/\nabla P_s$ of the resulting straight line was divided into the value of $\nabla I(0)/\nabla P_s$ calculated from Eq. 6 to give the inverse sensitivity $\nabla I/\nabla D$ of the detector. The results are presented in Table 2 (page 24).

When the detector block was cooled with liquid N_2, it was found that at I_b = 15.0 mA the thermal time constant of the filaments was intolerably long, wheras stability was bad at 30.0 mA. In the same manner as above the detector was calibrated for He^4 at T_d = 77°K (Table 2). The results show that at practical bridge currents the sensitivity at 77°K is almost four times that at 293°K.

TABLE 2

INVERSE SENSITIVITIES OF THE PIRANI DETECTOR WITH $K = 28$

GAS	T_d ^oK	I_b mA	V_b V	T_f ^oK	Measured $\nabla I/\nabla D$ mols/sec/ $cm^2/\mu V$
He^4	77	20.0	0.77	290	1.4×10^{12}
He^4	77	25.0	1.19	340	1.6×10^{12}
He^4	293	20.0	1.04	360	5.4×10^{12}
H_2	"	"	"	"	6.0×10^{12}
N_2	"	"	"	"	2.5×10^{12}
Ar	"	"	"	"	1.9×10^{12}

The ratio of these sensitivities is not the same as the ratio of the sensitivities of the Pirani gauge for the same pressure of these gases. This is because for a given beam intensity I, the cavity pressure P_d is not independent of the gas but depends on the molecular mass (Eq. 1).

(4) Sensitivity for He^3

From Eq. 1 it is evident that a given beam intensity of He^3 will produce a cavity pressure only $\sqrt{\frac{3}{4}}$ that produced by a He^4 beam of the same intensity. However, Eqs. 2 and 3 show that this smaller P_d will in fact produce the same voltage output, if the values of C_v and α are the same. Thus the measured sensitivities for He^4 are also valid for He^3, and

these can be compared with the theoretical sensitivities (page 11) if the latter are multiplied by the actual kappa-factor, $K = 28$.

TABLE 3

EXPERIMENTAL AND THEORETICAL SENSITIVITIES OF THE PIRANI DETECTOR

T_d °K	I_b mA	T_f °K	Measured VI/VD atoms/sec/cm^2/μV	He^3 Beam, I $\doteq 10^{13}$ atoms/sec/cm^2	
				Experimental Signal	Theoretical Max. Signal, T_f = 560K
293	20.0	360	5.4×10^{12}	1.9 μV	4.2 μV
77	20.0	290	1.4×10^{12}	7.1 μV	7.8 μV

Thus at practical bridge currents, the measured detector sensitivity was about 45% the theoretical maximum at room temperature, and about 90% the theoretical maximum at liquid-N_2 temperature. Hence the theoretical analysis gives a useful approximation of the performance of the Pirani detector.

(5) Conclusions

The output of the detector at room temperature for a He^3 beam of 10^{13} atoms/sec/cm^2 will be of the same order as the zero drift over a short period and with $P_v < 10^{-5}$ mm Hg, provided the detector has been outgassed. Of course the sensitivity could be increased by using entrance channels

of higher kappa-factor.

To compare the sensitivities of various Pirani detectors, it is necessary to extrapolate to $K = 1$ and measure intensities in mols/sec/cm^2, since K and the cross-sectional area of the entrance channel can be chosen arbitrarily. Table 4 lists the most sensitive Pirani detectors which have been described in the literature. Hydrogen is the only common gas for which all of these detectors have been calibrated.

TABLE 4

INVERSE SENSITIVITIES FOR H_2 OF PIRANI DETECTORS WITH $K = 1$

DETECTOR	T_d °K	VI/VD mols/sec/cm^2/μV
Ellett and Zabel, 1931	293	8.1×10^{14}
Kolsky et al, 1952	195	2.8×10^{15}
Present detector	293	1.7×10^{14}

Thus at room temperature the present detector is almost five times as sensitive for a H_2 beam as the previous most sensitive Pirani detector. This is largely because of the high surface area and resistance of the W-2 filaments.

Another considerable advantage of the present detector is the ease with which it can be fabricated, because of the convenient mounting of the W-2 filaments.

CHAPTER IV

DIRECTIVITY OF MOLECULAR BEAMS FROM CIRCULAR CYLINDRICAL TUBES

The following symbols are used frequently in this chapter:

ℓ = length of a circular cylindrical tube,

d = diameter " " " "

P_s = oven pressure,

P_v = residual gas pressure in the beam chamber,

λ_s = mean-free-path of the gas in the oven,

ℓ_{sd} = distance between beam source and detector inlet,

$\Delta\theta_{\frac{1}{2}}$ = full-width at half-maximum of a symmetrical angular distribution.

The flow through the tube is said to be molecular when $\lambda_s > \ell$ and viscous when $\lambda_s << d$.

A. Previous Measurements

Knudsen, 1909, and Mayer, 1929, experimentally verified the cosine law distribution of a neutral beam from an aperture ($\ell << d$) when $\lambda_s >> d$. A few directivity measurements, some of them inaccurate, with various tubes were made by Mayer, 1928 and 1929, Ellett, 1931, Korsunskii and Vekshinskii, 1945, Minten and Osberghaus, 1958, and Helmer et al, 1960. More extensive measurements were made by Gunther, 1957, using SiO_2 vapor and the precipitation-detection method. Naumov, 1963, has pointed out that Gunther's method involved serious sources of error and the investigation was incomplete, since Gunther

used only short canals ($\ell/d \leq 5$) and his measurements were restricted to $\theta \leq 45^{o}$. Nevertheless, his measurements indicated a limiting directivity pattern with $\Delta\theta_{\frac{1}{2}} = 76\text{-}79^{o}$ for any canal when $\lambda_s << d$.

Giordmaine and Wang, 1960, measured angular distributions of CO_2 beams from three sources, each consisting of an array of tubes with $\ell > 20d$; they examined only the region $\lambda_s < \ell$.

Naumov, 1963, has made the only thorough experimental investigation of beam directivities from tubes with $0.01 \leq \ell/d \leq 50$ and over a wide range of λ_s/ℓ for each tube. His experimental arrangement was similar to that shown in Figure 9. The gas used was ammonia. P_s was measured with a thermocouple gauge, while the beam detector was an ionization gauge used in conjunction with either a beam modulation device or a compensating gauge. Naumov's measurements disagree somewhat with Gunther's patterns, although Naumov did confirm a limiting $\Delta\theta_{\frac{1}{2}}$ of about 76^{o} for any tube when $\lambda_s \gtrsim 0.1\ d$.

Troitskii, 1962, has developed a theory of beam formation, and for the case of viscous flow he derived a limiting directivity pattern, $(\cos\theta)^{5/2}$ with $\Delta\theta_{\frac{1}{2}} = 80^{o}$. Troitskii's analysis was further developed by Ivanov and Troitskii, 1963, for the region $\lambda_s \geq \ell$, and their theoretical calculations are in good agreement with most of Naumov's results.

B. Apparatus

Figure 9 shows the experimental arrangement for obtaining directivity patterns. The beam source was rotated about a ver-

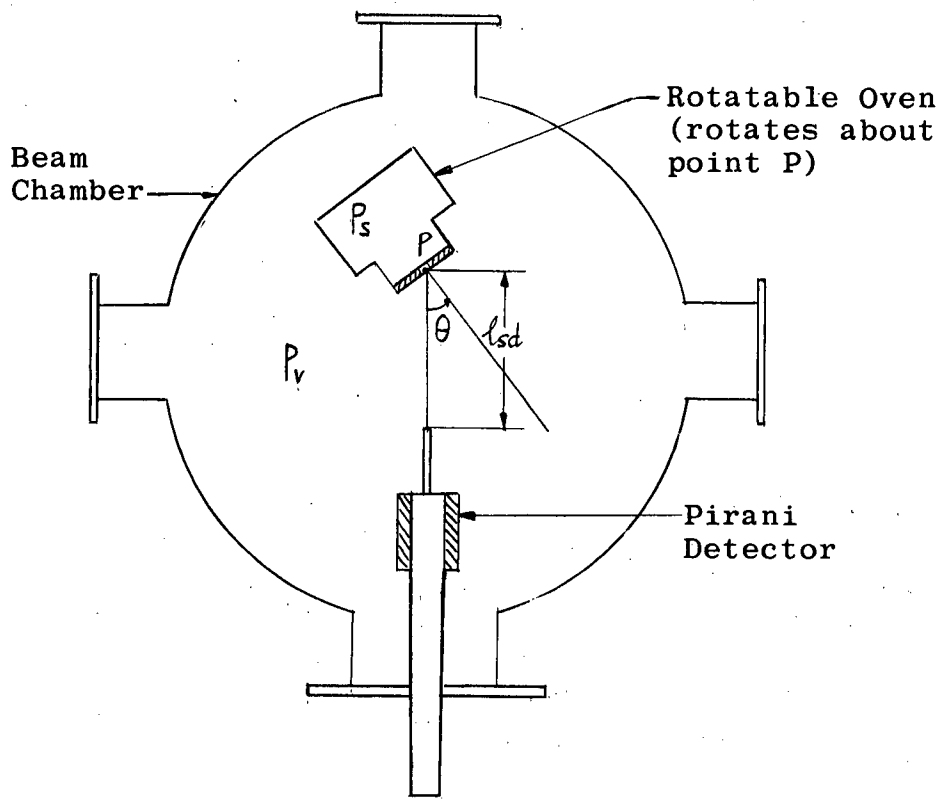

FIGURE 9. Experimental Arrangement for Measuring Angular Distributions of Molecular Beams.

tical axis through the center of the source face (point P), while the detector entrance channel, in the same plane as the source axis, was directed at P.

Figure 10 shows the rotatable beam-source which was positioned over the large port on the top of the beam chamber (Figure 7). Construction was mainly of brass, although the shafts were lengths of drill rod. The axis of rotation of shaft A was made to pass through the center of the tube face, perpendicular to the tube axis, by compressing the bellows and rotating the supporting post of the oven. A centering post was screwed into shaft A during this alignment. The shaft was turned with a worm gear, the amount of rotation being read on a scale fixed to the shaft.

The needle valve admitted gas to the oven through flexible 1/4" polyethylene tubing, B. P_S was measured with gauges connected to the oven with another piece of 1/4" flexible tubing, C, since for $P_S < 20$ microns there would in some cases be appreciable pressure drop along B. P_S was measured to at least 20% accuracy with the following gauges:

(a) 1 - 10 microns: Edwards Pirani gauge #M5B-2, calibrated against a McLeod gauge;

(b) 10 microns - 1 mm Hg: Edwards Vacustat #2E (miniature McLeod gauge);

(c) Above 1 mm Hg: Mercury manometer.

The oven could be rapidly pumped out through a 3/8" valve (D) connected to the beam chamber.

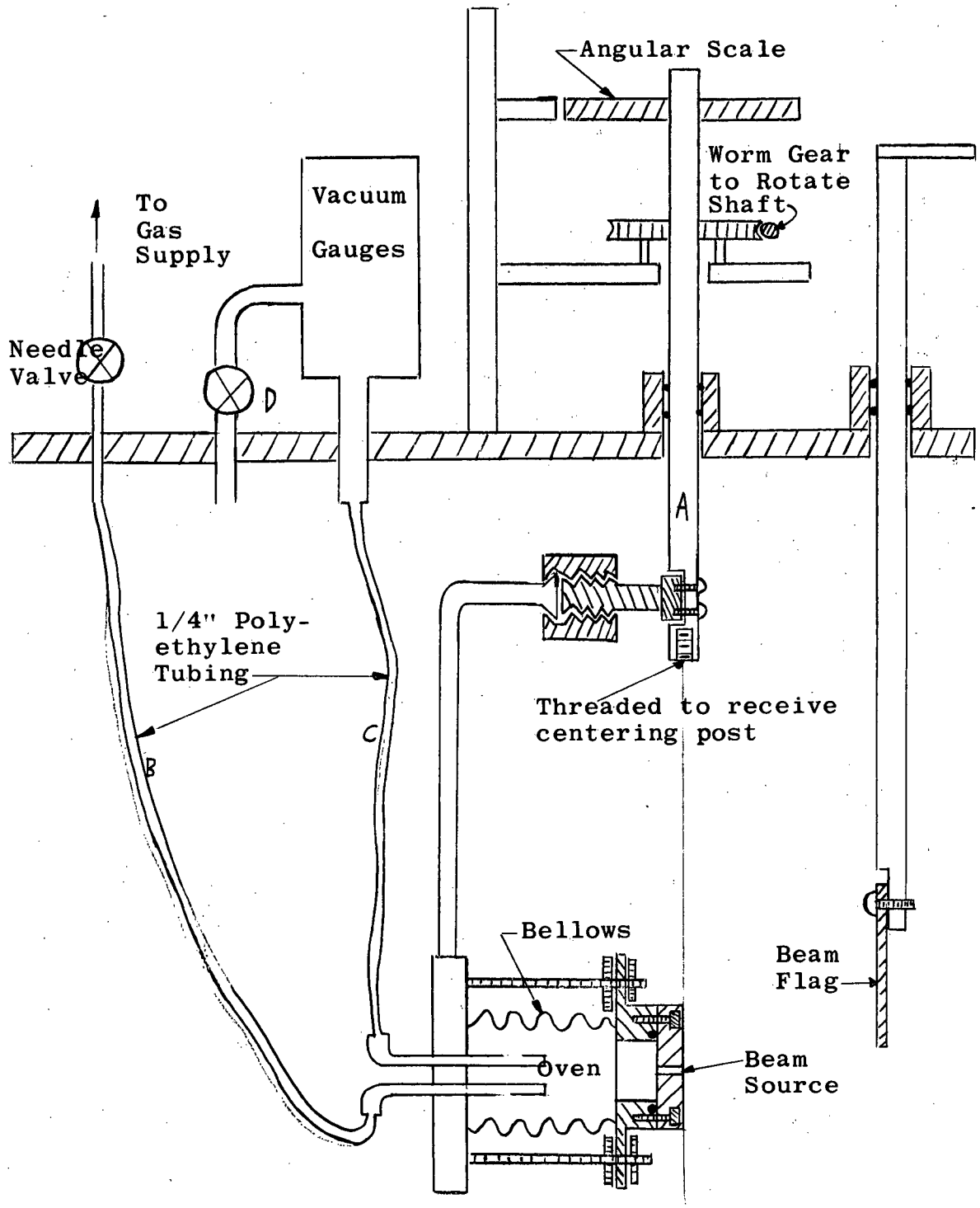

FIGURE 10. Schematic Diagram of the Rotatable Beam-Source.

C. Directivity Measurements

(1) Experimental Procedure

The reliability of the source-detector system was first investigated. The detector entrance channel was aligned with a 75-mm long 1/16" steel rod extending at right angles from the center of a flange positioned on the rotatable oven. This flange was then replaced with the 2-mm aperture (page 22), and the detector orientation adjusted until maximum signal was obtained for a molecular nitrogen beam produced by the aperture.

The angular distribution of the aperture beam was measured with P_s = 12 microns, so that for N_2, $\lambda_s/d = 2.1$. This distribution (Figure 11) was slightly narrower than the cosine distribution expected for an infinitely-thin aperture when $\lambda_s >> d$. This was because $d/\ell = 80$ rather than infinity; moreover, part of the aperture edge was slightly frayed which effectively made $d/\ell < 80$. Since $\lambda_s/d = 2.1$ rather than infinity, there were collisions in the aperture region which would narrow the beam. In view of these factors it was decided that the system was operating reliably.

Circular cylindrical channels were drilled in brass flanges which could be bolted to the rotatable oven. Table 5 lists the dimensions of the four tubes investigated. ℓ was measured with a micrometer, and d with a travelling microscope. The uncertainty in ℓ/d is less than 4% in all cases.

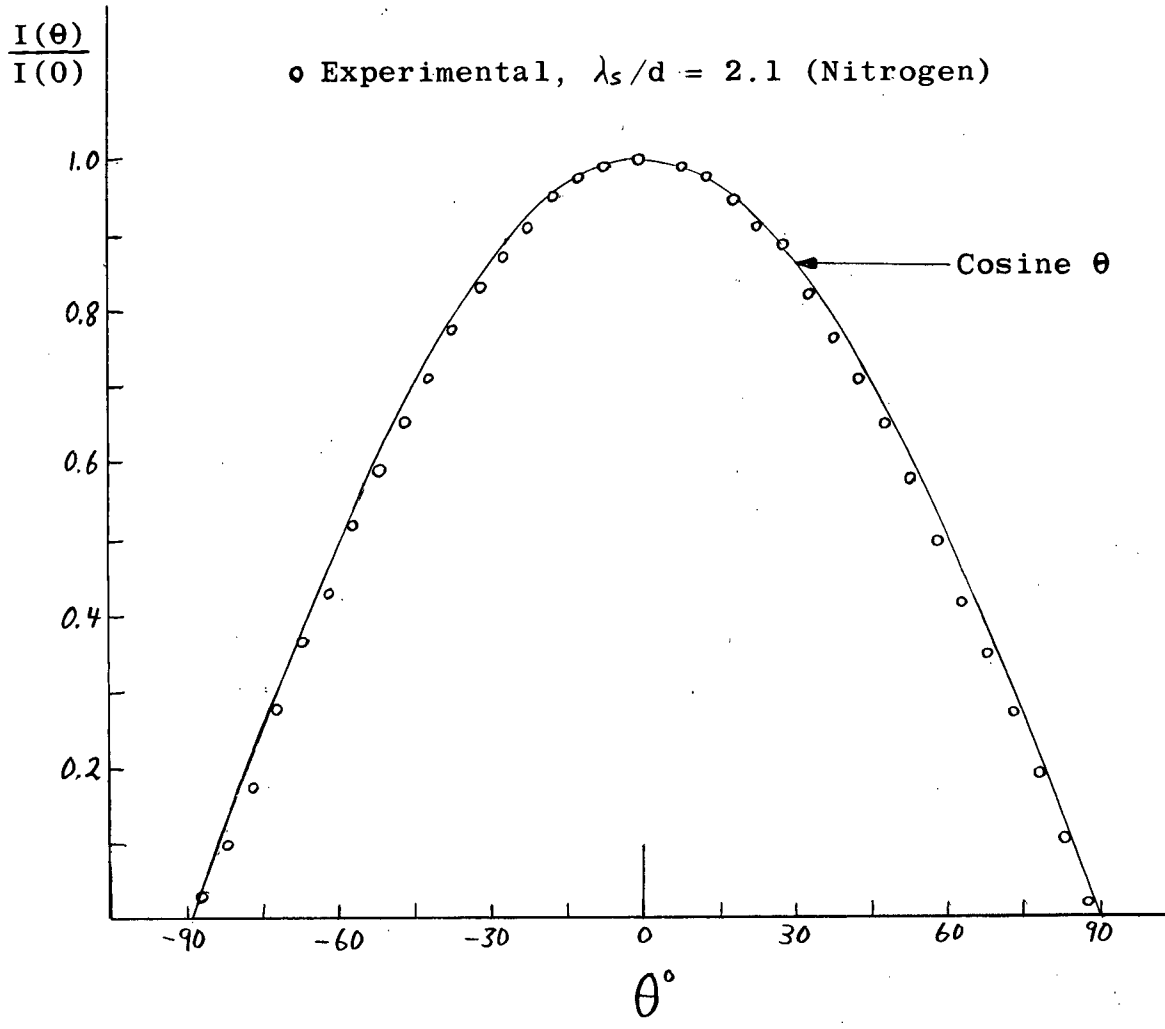

FIGURE 11. Angular Distribution of a Nitrogen Beam from the 2-mm Aperture.

TABLE 5

DIMENSIONS OF CIRCULAR TUBES

ℓ - mm	d - mm	ℓ/d
0.343	0.35	1.0
3.99	1.40	2.85
4.04	0.82	4.9
5.51	0.61	9.0

The diameters were so chosen that with $\lambda_s/\ell \geq 2$, $P_v \leq 10^{-5}$ mm Hg, so that detector drift was minimum, which was desirable for the small signal levels at the larger values of λ_s/ℓ. Naumov, 1963, investigated NH_3 beams from tubes with the same ℓ/d ratios (along with several others).

With each tube, ℓ_{sd} was chosen so that $d/\ell_{sd} << \Delta\theta_{\frac{1}{2}}$, as measured by Naumov,; this insured that the tube exit was effectively a point source. Final alignment of the detector was made as before. At each needle-valve setting, it was necessary to wait several minutes for P_s and P_v to reach equilibrium. The smallest P_s was such that reasonable beam intensity was obtained at the half-angles of the distribution, while the largest was such that the forepump could just keep the forepressure below the critical backing pressure of the diffusion pumps ($\sim$120 microns). Although detector drift was somewhat higher at relatively large P_v (10^{-4} to 10^{-3} mm Hg), the much higher detector signals produced by the intense beams made this drift insignificant. At any rate the beam flag was lowered before each reading

to check the detector zero.

At high P_v, no corrections for beam attenuation were necessary, since the angular distribution measurements involved only relative intensity. At each P_s, $\Delta\theta_{\frac{1}{2}}$ was found by rotating the source in each direction from the position of maximum intensity until the intensity was reduced by 50%. Complete angular distributions were measured only when $\lambda_s > \ell$.

(2) Results

In Figure 12 are plotted the measured values of $\Delta\theta_{\frac{1}{2}}$ as a function of λ_s/ℓ for the three gases used: helium, argon, and molecular nitrogen. λ_s was found by calculating λ_1/P_s, where λ_1 is the mean-free-path at 20°C and 1 micron. The following values of λ_1 were used (Dushman and Lafferty, 1962):
He - 145 mm; Ar - 52 mm; N_2 - 50 mm.

The results of Naumov, 1963, for NH_3 beams from tubes of about the same ℓ/d ratios are also plotted. When $\lambda_s/d > 0.1$, the present results show that $\Delta\theta_{\frac{1}{2}}$ is independent of the gas used at a given λ_s/ℓ ; however, the present values are somewhat smaller than those of Naumov.

In the viscous flow region, $\lambda_s/d \sim 0.1$, $\Delta\theta_{\frac{1}{2}}$ was found to be 75-79° for each gas and tube used, in agreement with the results of Gunther and Naumov. However, with increasing P_s $\Delta\theta_{\frac{1}{2}}$ does not remain constant at 76°; the angular distributions for Ar become narrower than those for N_2, presumably because a hydrodynamic jet is formed with a characteristic directivity

FIGURE 12. Measured F.W.H.M., $\Delta\theta_{\frac{1}{2}}$, of the Angular Distributions of Molecular Beams from Circular Cylindrical Tubes.

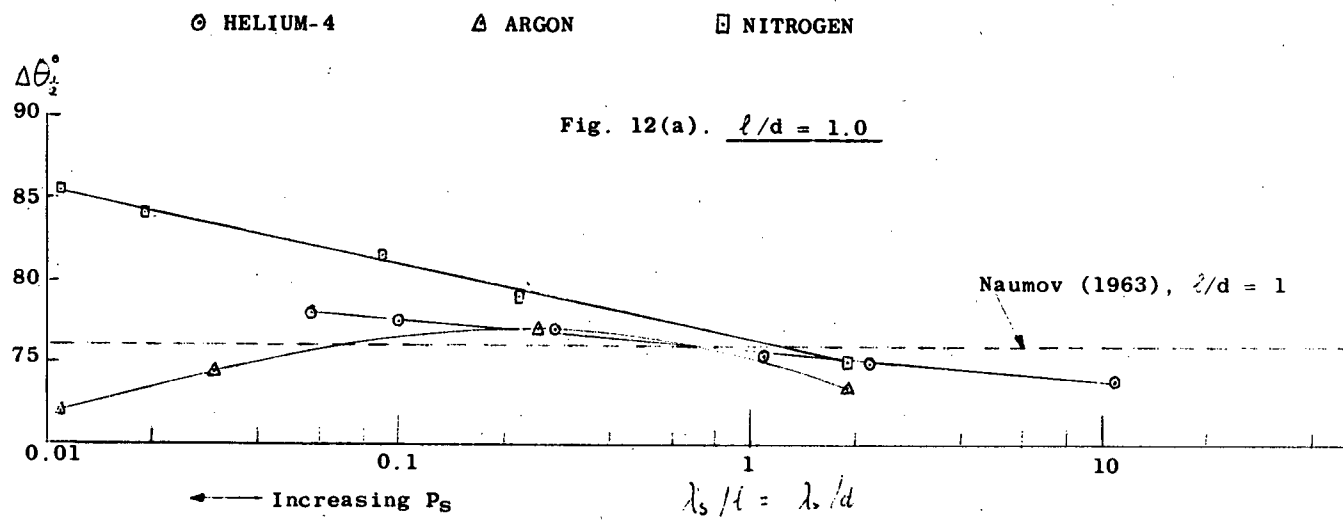

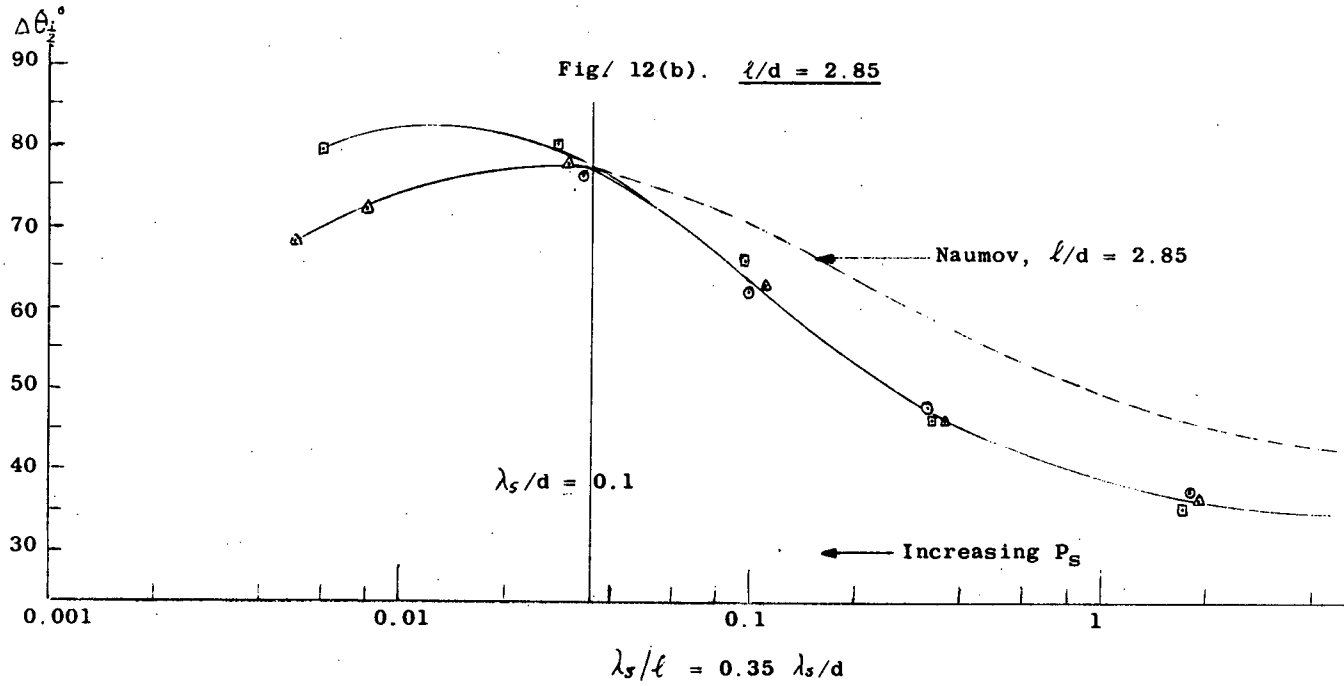

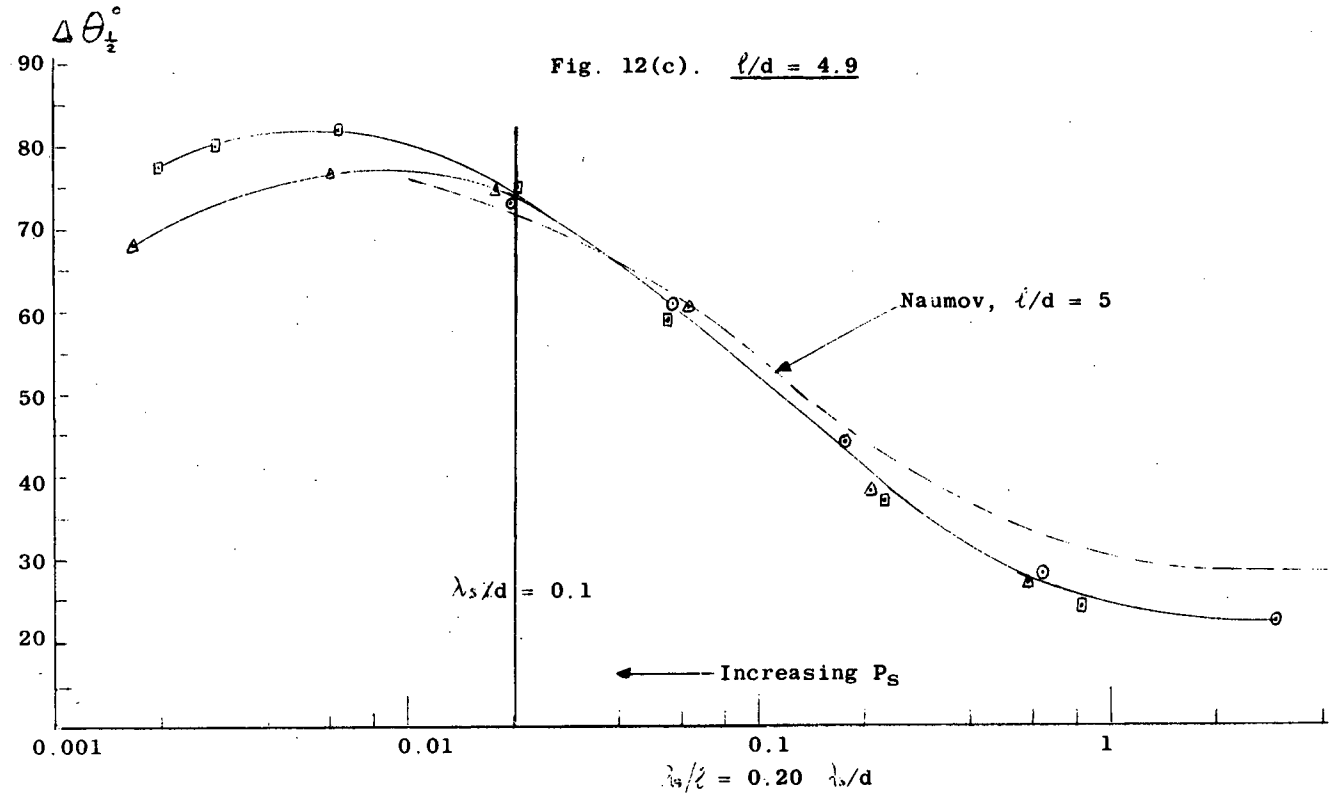

Fig. 12(c). $\ell/d = 4.9$

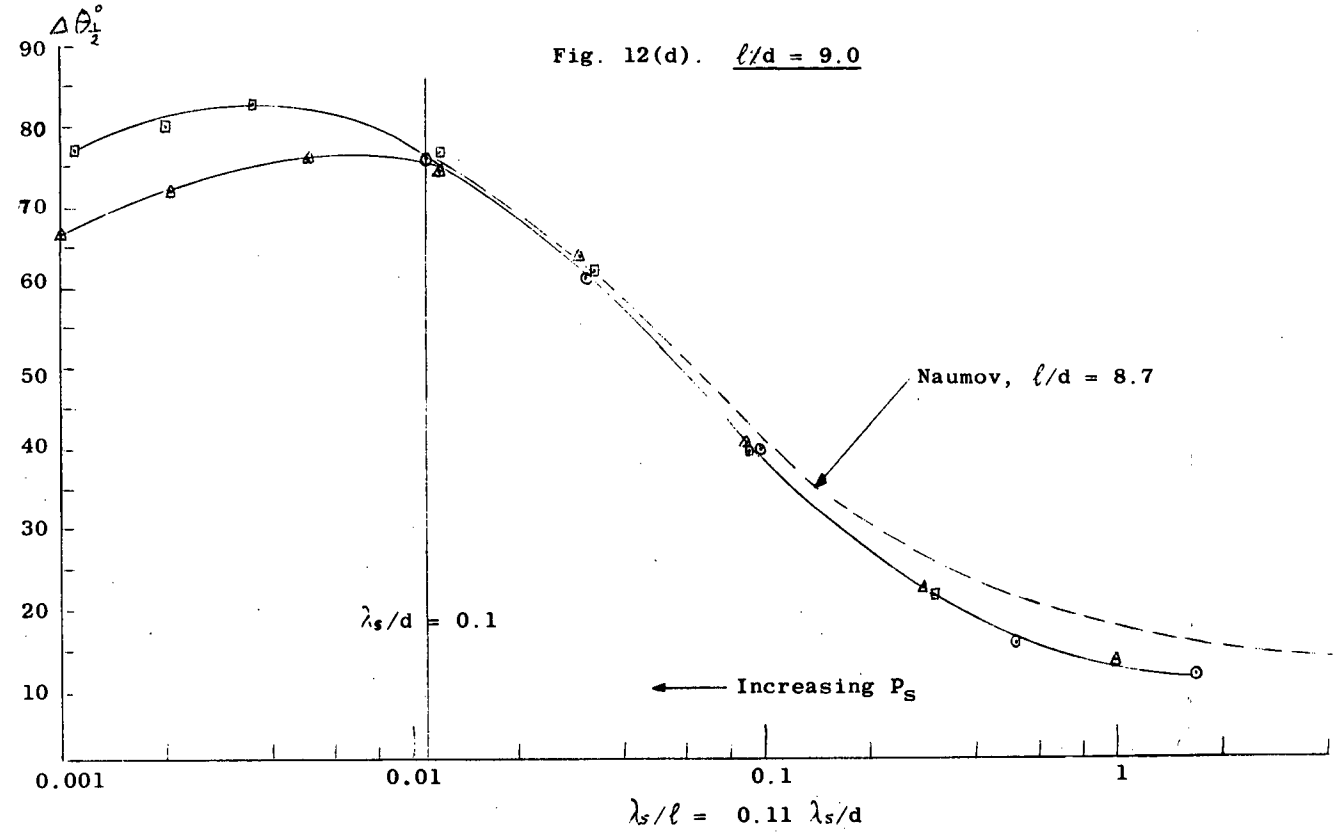

Fig. 12(d). $\ell/d = 9.0$

depending on the specific heat of the gas. These measurements may, however, be difficult to interpret accurately, since the effect of a boundary layer formed outside the tube exit in constraining the beam is not known. At the largest P_s, P_v was about 2 microns. The values of $\Delta\theta_{\frac{1}{2}}$ for He should be the same as those for Ar in this region, since their specific heats are the same; this could not be checked, however, since the flow rate for He was excessively large at $\lambda_s/d < 0.1$.

Complete angular distributions for He in the molecular-flow region are plotted in Figure 13. The measured distributions for Ar and N_2 were essentially the same.

Naumov's pattern for $\ell/d = 1$ has not been plotted, since it has $\Delta\theta_{\frac{1}{2}} = 94^o$, although in another section of his paper, Naumov maintains that $\Delta\theta_{\frac{1}{2}}$ is 76^o. For the other tubes, Naumov's distributions are somewhat wider than the present ones.

Gunther's distributions for $\ell/d = 1$ and 5 are in considerable disagreement with the present results as well as with those of Naumov. The theoretical distributions of Dayton, 1956, are based on the theory developed by Clausing (1930 and 1932). Dayton's pattern is too narrow for $\ell/d = 1$, but is a good fit when $\ell/d = 5$.

Troitskii's curves are plots of the equations

$$I_1(\theta) = I(0) \cos\theta \left(1 - \frac{\tan\theta}{2 \tan\theta_o}\right) \qquad \text{(Eq. 7)}$$

$$I_2(\theta) = I(0) \cos\theta \left(\frac{\tan\theta_o}{2 \tan\theta}\right) \qquad \text{(Eq. 8)}$$

where $\theta_o = \arctan d/\ell$

FIGURE 13. Angular Distributions of Molecular Beams from Circular Cylindrical Tubes in the Molecular-Flow Region ($\lambda_s > \ell$).

1 - Measurements of present author
2 - " " Naumov (1963)
3 - " " Gunther (1957)
4 - Theory of Troitskii (1962)
5 - " " Dayton (1956)

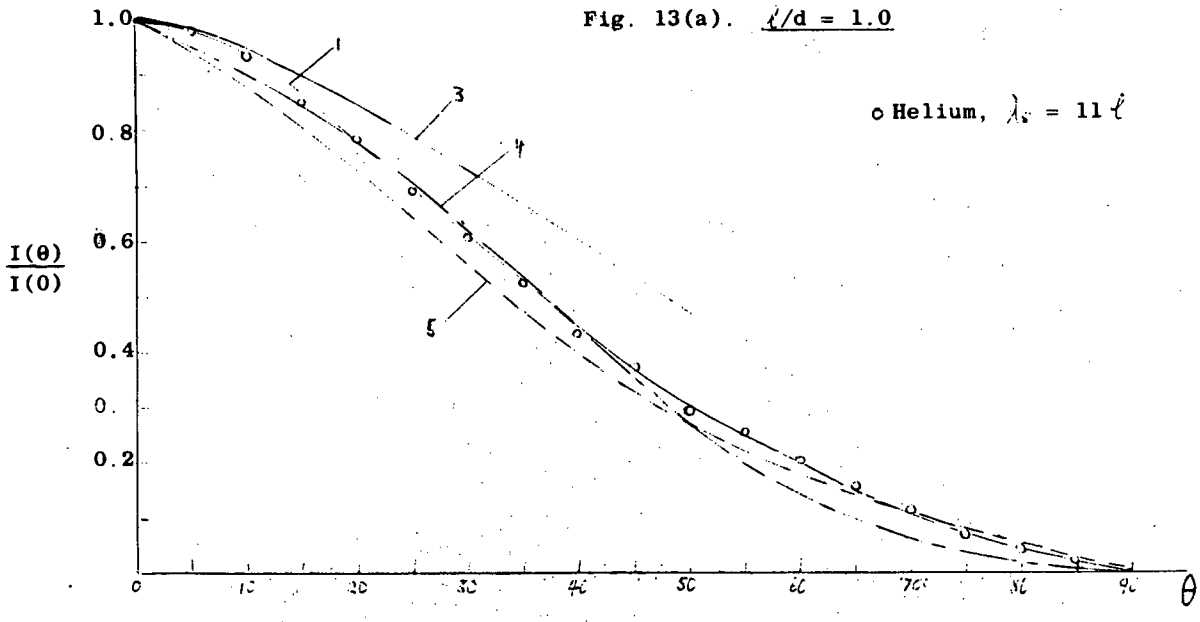

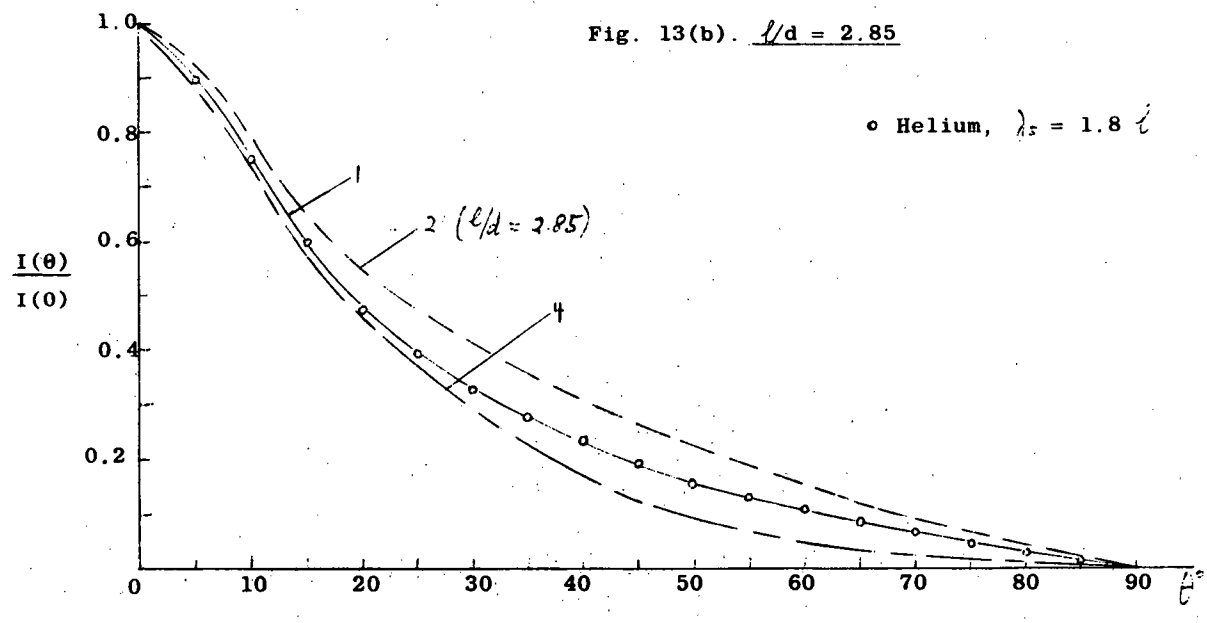

Fig. 13(c) $\ell/d = 4.9$

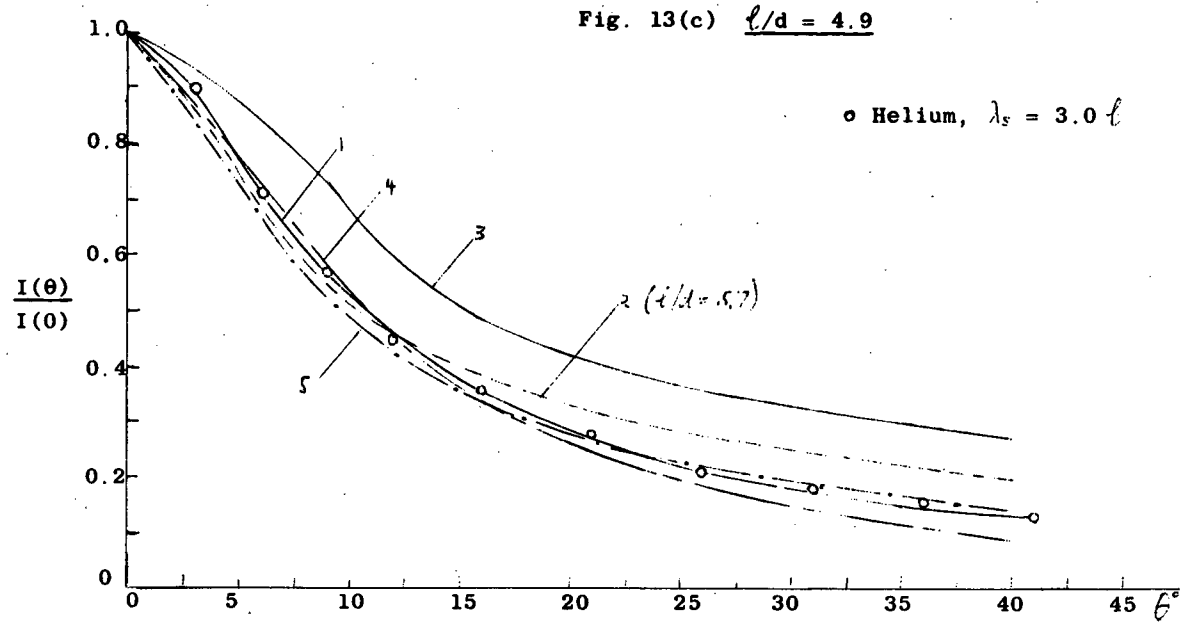

Fig. 13(d). $\ell/d = 9.0$

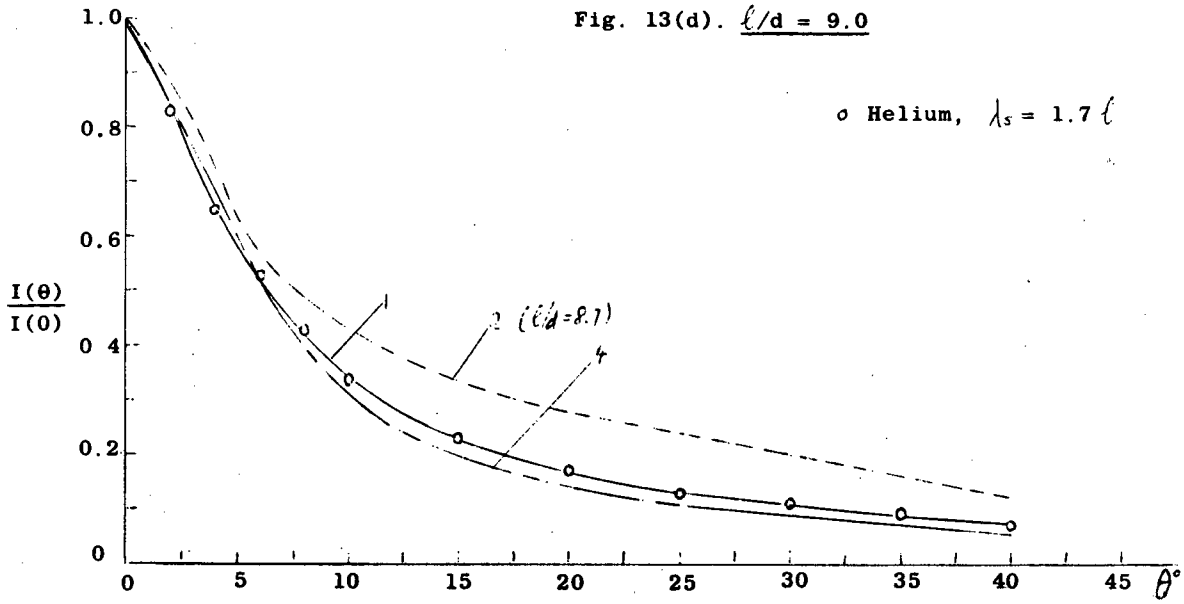

Troitskii, 1962, derived these equations from more general relations which he developed. For the latter he assumed, as do all the other theoretical treatments, that the reflection of molecules from any element of wall area is diffuse; i.e., according to a cosine distribution. The special assumption invoked to obtain Eqs. 7 and 8 is that the number of collisions per second of molecules with a given circular strip of the tube wall is directly proportional to the distance of the strip from the tube exit. The patterns calculated from Eqs. 7 and 8 fit the present distributions well for $I(\theta) > 0.4\ I(0)$, but fall too rapidly when $I(\theta) \leq 0.4\ I(0)$.

(3) Conclusions

The present results with helium, argon and nitrogen show that in the regions of molecular flow and the transition from molecular to viscous flow ($\lambda_s > 0.1d$), the angular distribution of the beam emerging from any circular tube is independent of the gas used, provided λ_s/ℓ is the same.

The present angular distributions are slightly narrower than those of Naumov, 1963. However, many of the dimensions of Naumov's tubes were given to only one significant figure with no mention of accuracy, so that it is perhaps meaningless to make a detailed comparison. Also, most of Naumov's results in Figures 12 and 13 were not taken with point sources, since except for $\ell/d = 1$, in order to increase the beam intensity, he used relatively large-diameter multichannel sources which did not always satisfy the condition $d/\ell_{sd} << \Delta\theta_{\frac{1}{2}}$. Although Naumov

stated that he averaged over the solid angle of the sources, Ivanov and Troitskii, 1963, apparently disregarded this and indicated that their theoretical directivity calculations did not agree well with some of Naumov's results because point-source conditions were not always realized.

However, it must be concluded that for most practical purposes Naumov's results for the fourteen tubes he measured are reasonably adequate.

If the present results are correct, then Troitskii's simple equations (Eqs. 7 and 8) can be used to compute the angular distribution for any tube in the molecular-flow region ($\lambda_s > \ell$) with good accuracy at those angles where the beam intensity is at least 40% maximum, and with fair accuracy outside those angles.

CHAPTER V

MACH NUMBER OF MOLECULAR BEAMS PRODUCED WITH A CONVERGING NOZZLE

A. Construction of Nozzles

The main component of the atomic beam source in the polarized helium-3 apparatus is a 0.20-mm (0.008") diameter nozzle which must produce a Mach 4 beam with a pressure ratio across the nozzle of $\sim$100 (Axen, Klinger and Warren, 1963). The theory of gasdynamics shows that sonic flow is attained at the throat of a nozzle, and supersonic flow can be achieved only if the gas expands further in the diverging section of a converging-diverging or Laval nozzle (see e.g., Shapiro, 1953). However, Becker and Bier, 1954, and Deckers and Fenn, 1963, have reported that supersonic flow can be achieved with simple converging nozzles, presumably because immediately outside the nozzle exit an expanding boundary layer is formed, taking the place of the diverging section of a Laval nozzle. After some trials, because of the relative ease of manufacture, it was decided to attempt to build a suitable converging rather than Laval nozzle.

The nozzle shape chosen was that of a simple cone (Figure 14). Nozzles of this shape were manufactured of brass, nickel-babbitt and aluminum by the following methods.

With brass and aluminum a conical hole was first cut out of the metal with a steel cutter of total included angle 40°

Scale: 3:1

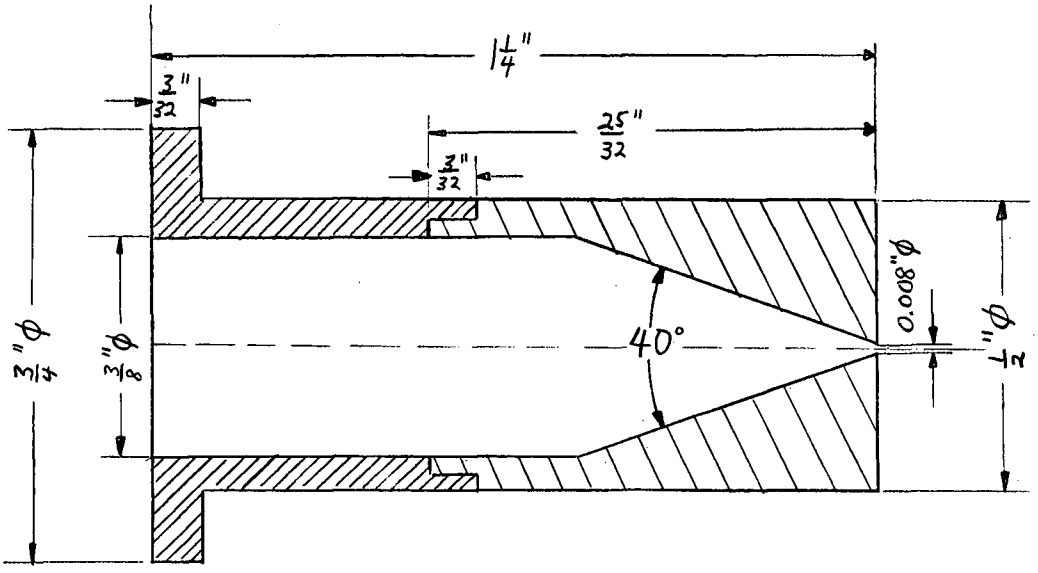

FIGURE 14. Conical Converging Nozzle and Holder

(20^{o} taper). The metal was then centered in a lathe and machined from the side opposite the cone opening until a tiny hole just appeared, typically about 0.006" diameter, but not perfectly round. The hole was rounded with a steel needle which increased the diameter to about 0.008". This method was found superior to using an 0.008" drill, which invariably produced an imperfect hole.

With Nickel-babbitt the 20^{o} cutter was used to cut only a section of a cone with minimum diameter about 3/16". Since Ni-babbitt is a soft metal, the remaining part of the cone was produced by pushing a carefully-polished, conically-shaped tool-steel bit into the metal with a hammer. The 0.008" hole was produced as above.

The nozzles were mechanically polished with a suitably shaped piece of wood coated with rouge or fine polishing grit (alundum). One aluminum nozzle was chemically polished by immersion for 30 sec in the following polishing solution, heated to 200^{o}F: 75% phosphoric acid (1.70 sp.gr.) by wt.; 3.5% hydrogen peroxide (30%) by wt.; 21.5% water by wt.

The diameters of the nozzle exits were measured with a travelling microscope to better than 2% accuracy.

B. Measurement of Flow Rate

For both Laval and converging nozzles, the theoretical mass flow rate through the nozzle is given by (Shapiro, 1953)

$$G = A \left(\frac{2}{\gamma+1}\right)^{\frac{1}{\gamma-1}} \sqrt{\frac{2\mu\gamma}{(\gamma+1)R}} \frac{P_s}{\sqrt{T_s}} \qquad \text{(Eq. 9)}$$

where A = minimum cross-sectional area of the nozzle,

γ = ratio of the specific heats of the gas,

μ = molecular weight of the gas,

R = molecular gas constant,

P_S = pressure of the gas in the source chamber (oven),

T_S = temperature " " " " " " "

Eq. 9 is valid when the pressure ratio across the nozzle

$$\frac{P_s}{P_v} > \left(\frac{2}{\gamma+1}\right)^{\frac{\gamma}{1-\gamma}} \quad \text{or} \quad \frac{P_S}{P_v} > 2.1 \text{ for } \gamma = 1.67;$$

Moreover, the flow through the nozzle must be one-dimensional (i.e., uniform across each section), isentropic, frictionless, and free of turbulence. Becker and Bier, 1954, verified that Eq. 9 is valid within 5% for nozzles of throat diameter $\sim$0.5mm.

For He^4 at 20°C, Eq. 9 reduces to 445 P_S d^2 micron-liters per second, where d is the smallest diameter of the nozzle in mm, and P_S is the oven pressure in mm Hg. Thus for d = 0.20 mm and P_S = 20 mm Hg, the theoretical flow is 356 μ-ℓ /sec.

The flow rates through the converging nozzles were measured by the method described in Appendix C. Figure 15 shows the measured flow rates for some of the nozzles tested, expressed as a percentage of the theoretical flow rate given by Eq. 9. Tests with a 1.1-mm brass nozzle indicated that for optimum performance the nozzle surface, particularly near the exit, must be clean and well-polished. The smallest brass and nickel-

FIGURE 15. Flow of Helium-4 through some Conical Converging Nozzles at 20°C.

● Brass nozzle, well-polished, d = 1.09 mm.
□ Aluminum nozzle, before chemical polishing, d = 0.205 mm.
○ " " after " " d = 0.214 mm.
△ Nickel-babbitt nozzle, mechanically polished, d = 0.282 mm.
▲ Brass nozzle, no polishing, d = 0.158 mm.

All nozzles were cleaned with acetone.

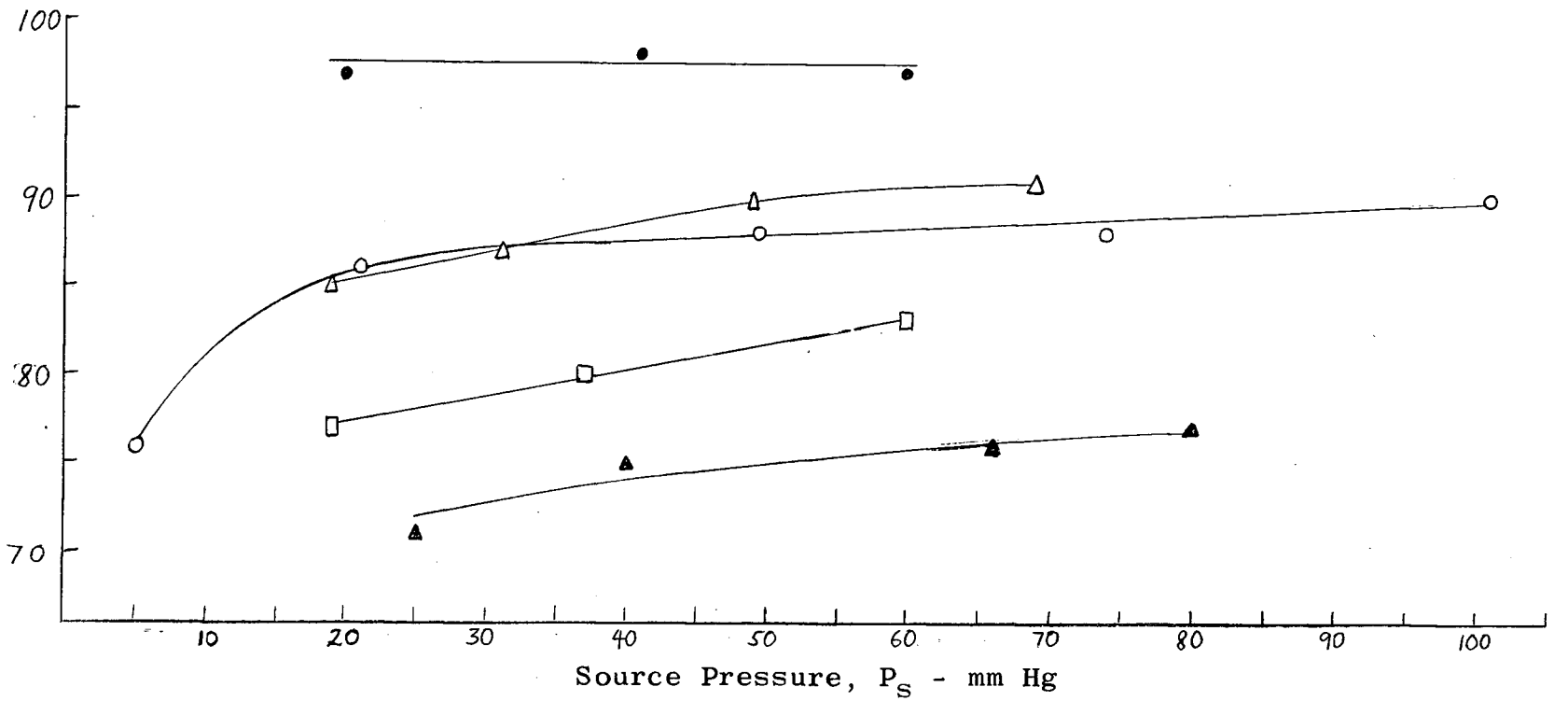

babbitt nozzles performed inadequately, probably because of considerable dirt and surface imperfections near the nozzle exit which could not be removed by mechanical polishing without seriously enlarging the exit diameter (to 0.28mm or more). The flow rate through the 0.214-mm chemically-polished aluminum nozzle, however, was reasonably satisfactory, so that it was decided worthwhile to attempt to measure the Mach number of the beam it produced.

C. Measurement of the Mach Number

(1) Interpretation of Impact-pressure Measurements

In experimental gasdynamics, the Mach Number, M, of a gas stream is usually measured with a Pitot tube, a small-diameter tube one end of which is open and aligned parallel to the flow, facing the upstream direction, while the other end is connected to a pressure gauge. Becker and Bier, 1954, used a Pitot tube with I.D. = 0.35 mm and O.D. = 0.60 mm to measure M of a molecular hydrogen beam produced with a 0.5-mm Laval nozzle.

M is found from one of the following formulas (Shapiro, 1953):

(a) Subsonic flow: $$\frac{P_P}{P_1} = \left(1 + \frac{\gamma-1}{2} M^2\right)^{\frac{\gamma}{\gamma-1}} \qquad \text{(Eq. 10)}$$

(b) Supersonic flow: $$\frac{P_P}{P_1} = \left\{\frac{(\gamma+1)^{\gamma+1}\, M^{2\gamma}}{2^{\gamma}\left[2\gamma M^2 - (\gamma-1)\right]}\right\}^{\frac{1}{\gamma-1}} \qquad \text{(Eq. 11)}$$

P_p is the impact pressure, the pressure indication of the gauge attached to the Pitot tube. P_1 is the static pressure

or pressure in the gas stream, and in the following measurements P_1 was taken to be the pressure P_v in the beam chamber, since presumably the gas emerging from the nozzle expands to this pressure (Becker and Bier, 1954). Eqs. 10 and 11 are plotted in Figure 16, for $\gamma = 1.67$.

(2) Modification of the Differential Pirani Detector

The entrance channel of the Pirani detector was small enough to be used successfully as a Pitot tube (I.D. = 0.80 mm and O.D. = 1.0 mm). The filaments in the beam cavity acted as the pressure-sensitive elements of an ordinary Pirani gauge, while the filaments in the compensating cavity were not used.

The circuit diagram of this Pirani gauge is shown in Figure 17. The two ranges enabled the Wheatstone bridge to be conveniently balanced over the entire practical range of filament resistance (41-95 ohms).

The gauge was calibrated for both He^4 and Ar. A typical calibration curve is shown in Figure 18. In this case the bridge current was set at 125 mA with a beam-chamber pressure of 500 microns. The gauge output was then recorded for various pressures between 10 microns and 10 mm Hg, as measured by the miniature McLeod (vacustat) or mercury manometer.

(3) Impact-Pressure Measurements on Beams from the 0.214-mm Converging Nozzle.

These measurements were taken with the beam chamber pumped only with the mechanical pump, since with He^4 at

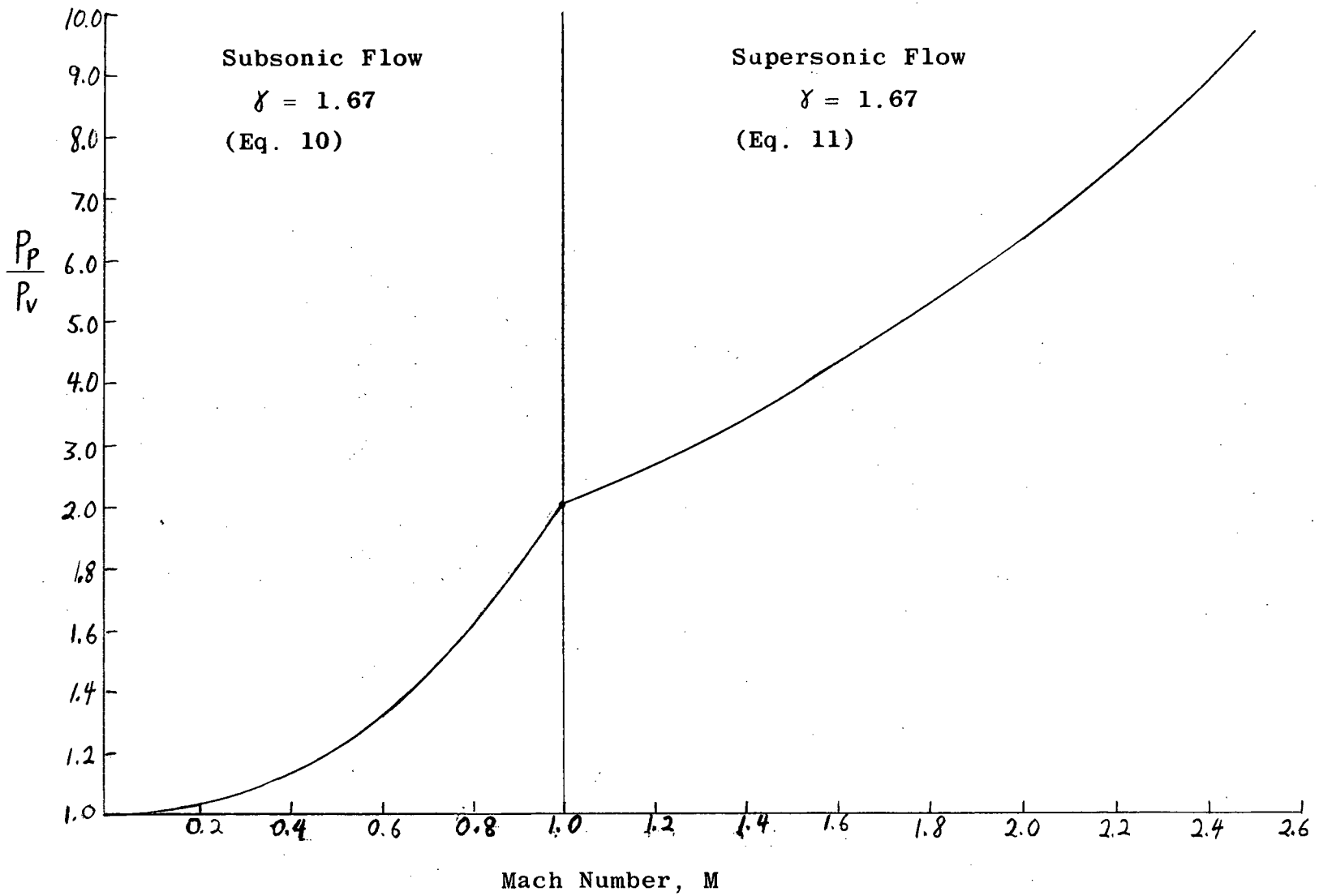

FIGURE 16. Stagnation-Pressure Rise in Pitot Tube vs Mach Number of Gas Flow.

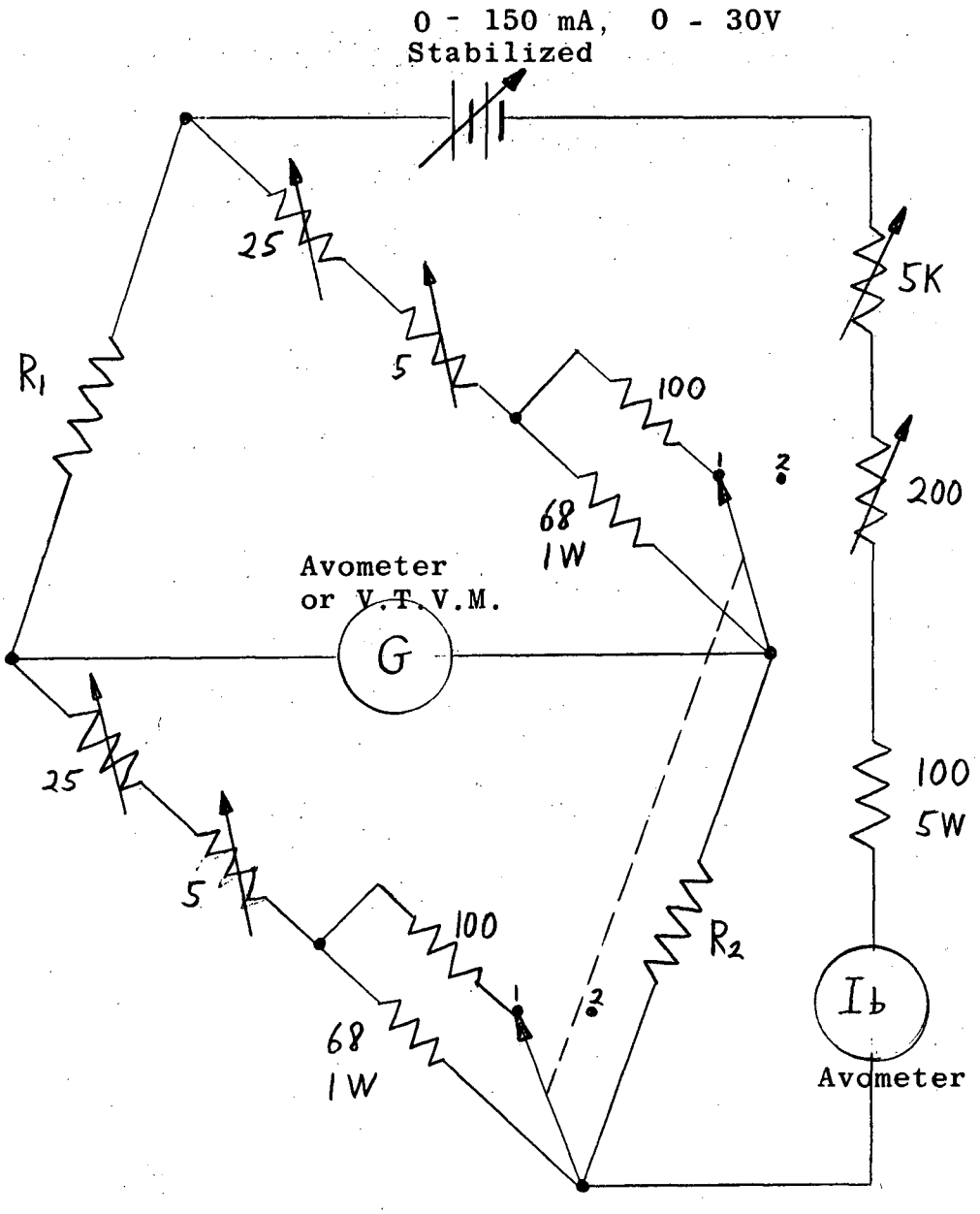

R_1 and R_2 are the Pirani Filaments (Gow-Mac Type W-2).

Resistances in ohms. Resistors 5% and 1/2 watt, except where otherwise noted.
Potentiometers wirewound and 5 watt.

FIGURE 17. Circuit Diagram for the Pirani Gauge.

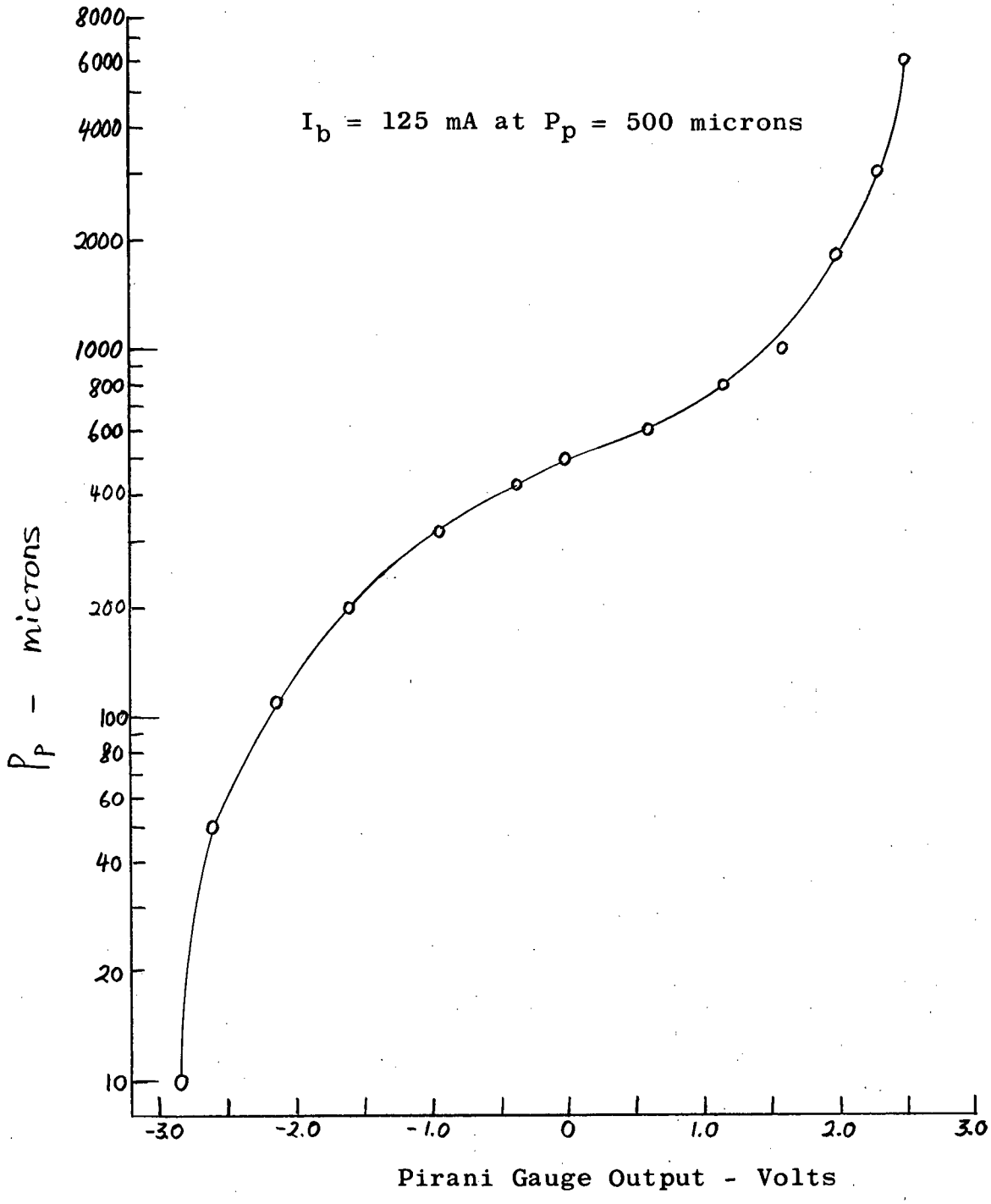

FIGURE 18. Calibration Curve for Pitot-Tube Pirani Gauge, for Helium-4.

P_s > 15 mm Hg the mechanical pump could not keep the fore-pressure below the critical backing pressure of the diffusion pumps. Moreover, Eq. 11 is in considerable error when the gas density about the Pitot tube is extremely low(< 50 microns; Devienne, 1960).

The 0.214-mm converging nozzle was attached to the rotatable oven so that the Pitot tube could be brought right up to the nozzle exit. At each nozzle-tube distance ℓ_{sd} , P_s was set arbitrarily and the tube carefully aligned for maximum Pirani signal. Then for each of a number of values of P_s, the static pressure P_v was read with the vacustat and the Pirani output converted to the impact pressure P_p by means of the suitable calibration curve. M was found from Figure 16.

Figure 19 shows M for several helium-4 beams at distances up to 10 mm from the nozzle. In each case the pressure ratio across the nozzle was 120 to 125. These curves are exponential on a linear plot. M decreases with increasing ℓ_{sd} because of energy loss of the beam by collision with the surrounding gas. The three curves when extrapolated indicate a Mach number of about 2.2. at the nozzle exit.

At an expansion ratio of 120, a perfect Laval nozzle would produce a Mach 4.1 beam, according to the formula (Shapiro, 1953)

$$\frac{P_v}{P_s} = \left\{\frac{2}{2 + M^2(\gamma-1)}\right\}^{\frac{\gamma}{\gamma-1}} \qquad \text{(Eq. 12)}$$

Similar curves for Argon at an expansion ratio of 300

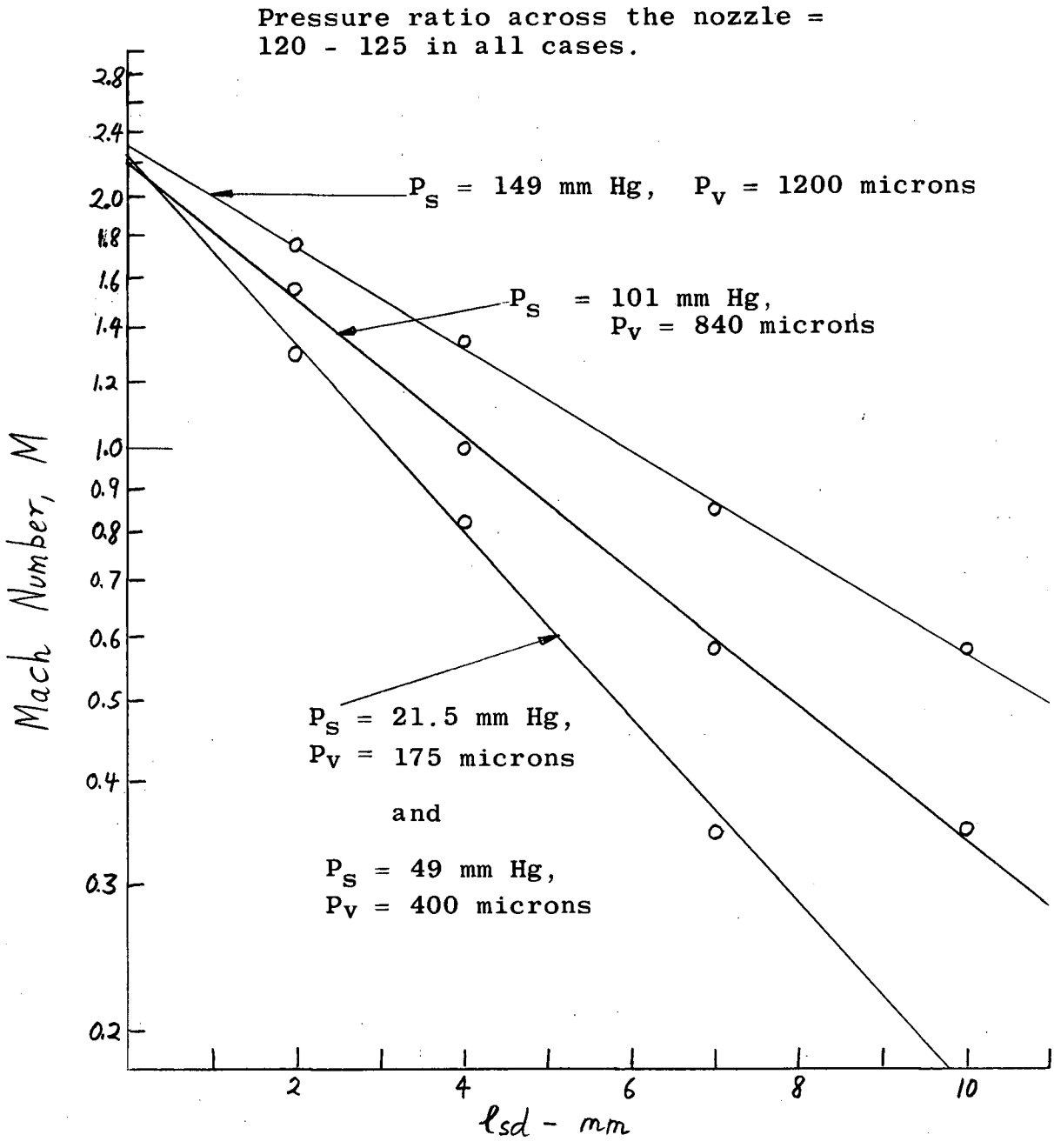

FIGURE 19. Pitot-Tube Measurements of Mach Numbers of Helium-4 Beams from the 0.214-mm Conical Converging Nozzle.

indicate a Mach number only slightly higher — about 2.5. The pressure ratio across this nozzle, if used at 2.2°K in the polarized He^3 apparatus, will be about 150 (10 mm Hg / 70 microns), so one would expect a Mach 2.3 beam.

CHAPTER VI

SOME FURTHER ASPECTS OF BEAMS PRODUCED WITH THE CONVERGING NOZZLE

A. Nature of the Measurements.

If a nozzle is mounted on the rotatable oven and a high source pressure maintained, the relative detector signal as a function of the angular displacement θ of the oven will not in general be a measurement of the portion of the beam (relative number of mols/sec/cm^2) which emerges from the nozzle in the direction defined by θ. For example, at large post-nozzle pressures, $P_v > 50\mu$, the gas in the detector cavity and entrance channel forms a continuum, so that the Mach number of the beam rather than intensity is measured.

At $2\mu < P_v < 50\mu$, the gas in the detector is partly in a continuum state and partly in a state of free-molecular flow. At any rate this range cannot be investigated with the present apparatus, since the backing pressure of the diffusion pumps is intolerably high at $P_v > 2\mu$, and with the forepump alone, $P_v = 50\mu$ corresponds to a source pressure of only 15 mm Hg, for argon.

In the region $P_v < 2\mu$, free-molecular flow exists in+about the Pirani detector, so that the detector actually measures beam intensity. However, since the nozzle beam is shaped by the boundary layer formed outside the nozzle exit, the measured angular distribution will not in fact correspond to the actual

directivity of the core of the beam as it emerges from the plane at which the beam has fully expanded. Because of this shaping effect of the boundary layer, molecules at some distance from the nozzle axis may actually be travelling parallel to the axis, and yet strike the detector at some angle θ and be recorded. Moreover, the intensity of pressure waves evaporating from the boundary layer will also be measured.

At any rate, the range $P_v < 2\mu$ is not a useful one to investigate, since the beam-shaping effect of the boundary layer at $P_v \sim 1\mu$ is probably vastly different from its effect at $P_v \sim 100\mu$, the region of interest. Also, the expansion ratio at $P_v \sim 1\mu$ is unrealistically high, about 30,000 for argon.

We consider, then, only the region $P_v > 50\mu$.

Eq. 10 gives the Mach number, M, of the beam as a function of Pitot pressure P_p and static pressure P_v, for $M < 1$. This equation can be written as a series (Liepmann and Roshko, 1957):

$$P_p = P_v + \tfrac{1}{2}\rho v^2 \left(1 + \frac{M^2}{4} + \cdots\right) \qquad \text{(Eq. 13)}$$

where ρ is the density (mass per unit volume) of the gas and v the velocity in the stream immediately in front of the Pitot tube.

With <10% error if $M < 0.6$ and <20% error if $M < 0.9$, we can write Eq. 13 as

$$P_p - P_v \approx \tfrac{1}{2}\rho v^2 \qquad \text{(Eq. 14)}$$

Thus for $M < 0.9$, the Pitot-tube pressure, after subtracting the static pressure, is a rough measure of the directed kinetic-energy density of the beam at the point of measurement.

The detector signal for angular displacement θ of the oven will be a rough measure of the directed kinetic-energy density at point B, displaced $\ell_{sd} \sin\theta$ from point A on the nozzle axis, whose distance from the nozzle exit, b, is approximately ℓ_{sd} (Figure 20).

An error is introduced into this measurement due to the fact that the Pitot tube will probably not be pointing in the stream direction at point B, which is unknown and could, for example, be parallel to the nozzle axis, because of boundary-layer shaping. This error is probably not serious, however, since Pitot-tube measurements are usually not critically dependent on alignment of the tube with the stream direction. With a simple open-ended tube, in fact, only 1% error results from a misalignment of 20° in the plane of the flow (Liepmann and Roshko, 1957).

Thus, the curve of relative detector signal due to the nozzle beam vs angular displacement of the oven is a rough indication of the spatial distribution of the directed kinetic energy of the beam. This curve is symmetrical about $\theta = 0^{\circ}$, and we denote by -FW- the full-width at half-maximum.

In experimental gasdynamics, it is common to investigate the profile of a nozzle beam by moving a Pitot tube across the beam (perpendicular to the flow direction) by means of a suitable micrometer drive.

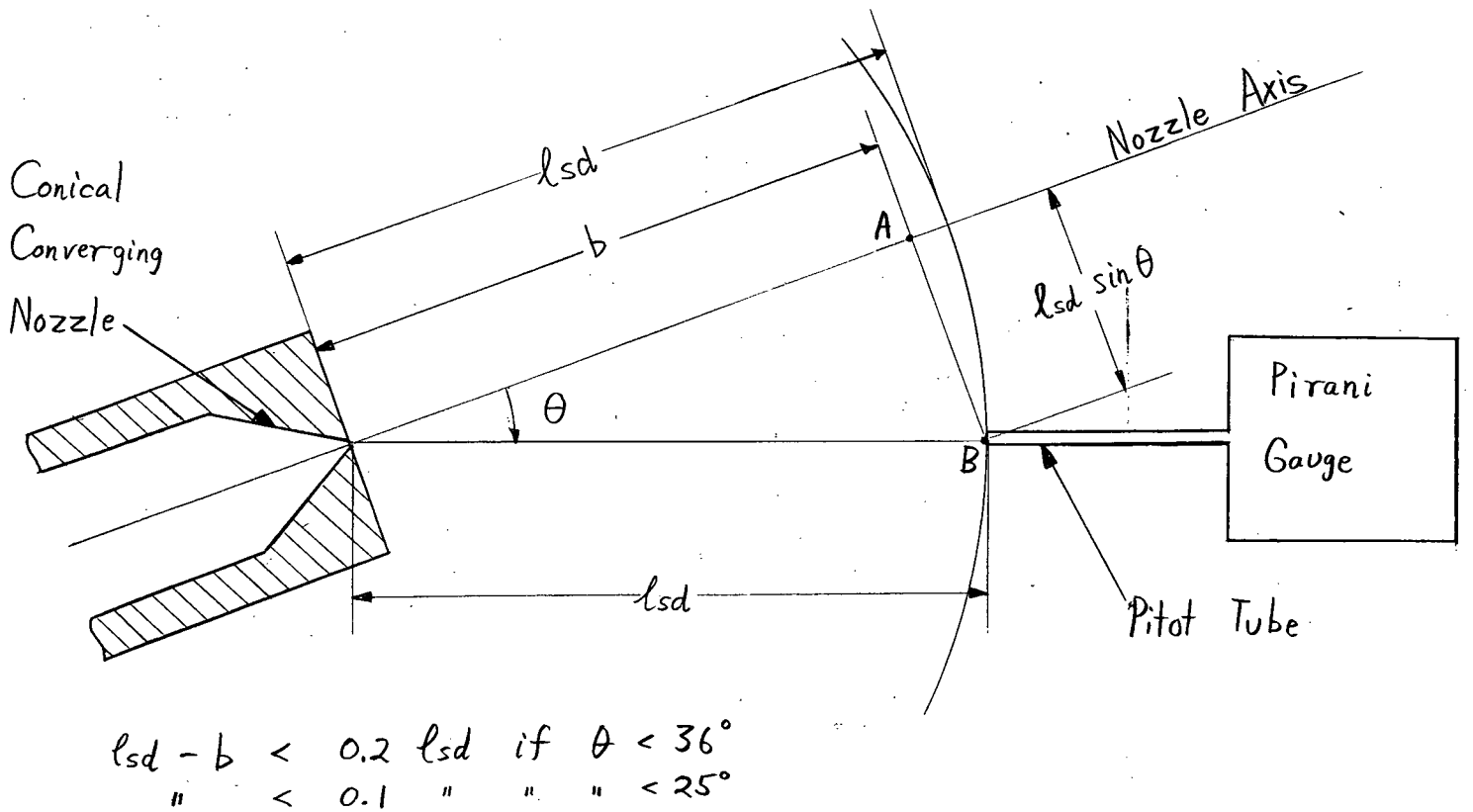

The direction of flow at point A is parallel to the nozzle axis.
" " " " " " B " unknown.

FIGURE 20. Geometry of the System for Probing Nozzle Beams.

B. Experimental Procedure

The experimental arrangement was that shown in Figure 9, with the nozzle bolted to the rotatable oven. The detector was operated as a simple Pirani gauge (page 40). The gauge was calibrated for argon in the range P_v = 30 to 2000 microns at various I_b from 40 to 110 mA. However, the calibration was carried out only roughly, since it was desired only to locate linear operating regions. For measuring relative pressures, a linear response was convenient, and absolute values were not of interest.

At a given ℓ_{sd}, the detector was carefully aligned with the nozzle beam for maximum detector signal ($\theta = 0^o$). At a given P_s and P_v, the Wheatstone bridge was balanced with the beam flag down. I_b was chosen so that with the beam flag up, at $\theta = 0^o$ the detector signal corresponded to a pressure on the same linear region of the calibration curve containing the pressure corresponding to the detector signal with the beam flag down. This insured a linear response to pressure at all θ. Since the bridge was balanced with the beam flag down (gauge pressure = P_v), the detector signal at any angle was proportional to $P_p - P_v$, or approximately $\frac{1}{2}\rho v^2$ (Eq. 14).

FW was found by turning the oven in both directions from the position of maximum signal until the signal was reduced by 50%. Mach numbers were measured as explained in Ch. V. ℓ_{sd} was always sufficiently large that $M < 0.9$, so that Eq. 14 was valid to at least 20% accuracy.

C. Results

Figure 21 shows the FW for an argon beam at constant P_s, but with P_v varied by admitting argon via a needle valve. The curve shows that at point B (Figure 20), the directed kinetic-energy density of the beam relative to that at point A decreases exponentially with increasing residual gas pressure, if A is a considerable distance from the nozzle exit (ℓ_{sd} = 36 mm). Of course, the Mach number of the beam at the nozzle exit presumably decreases with increasing P_v, since P_s is constant.

Figure 22 shows the FW at ℓ_{sd} = 36 mm for argon beams at various P_s, but with P_s/P_v fairly constant, so that the Mach number at the nozzle exit is presumably the same for each beam ($\sim$2.5). Again, at point B, the directed kinetic-energy density of the beam relative to that at point A decreases exponentially with increasing P_v, even though, as Figure 19 shows, at higher P_s and thus higher P_v, the directed kinetic energy at point A is a larger fraction of the directed kinetic energy of the same beam at the nozzle exit.

Figures 23 (a) and (b) show in two particular cases how the detector signal $D(\theta)$ due to the beam varies as a function of the angular displacement θ of the oven. Since the Mach numbers of the two beams are less than 0.9 on the nozzle axis at these ℓ_{sd}, the curves show roughly how the directed kinetic-energy density of the beam varies as a function of the displacement $\ell_{sd}\sin\theta$ from the nozzle axis.

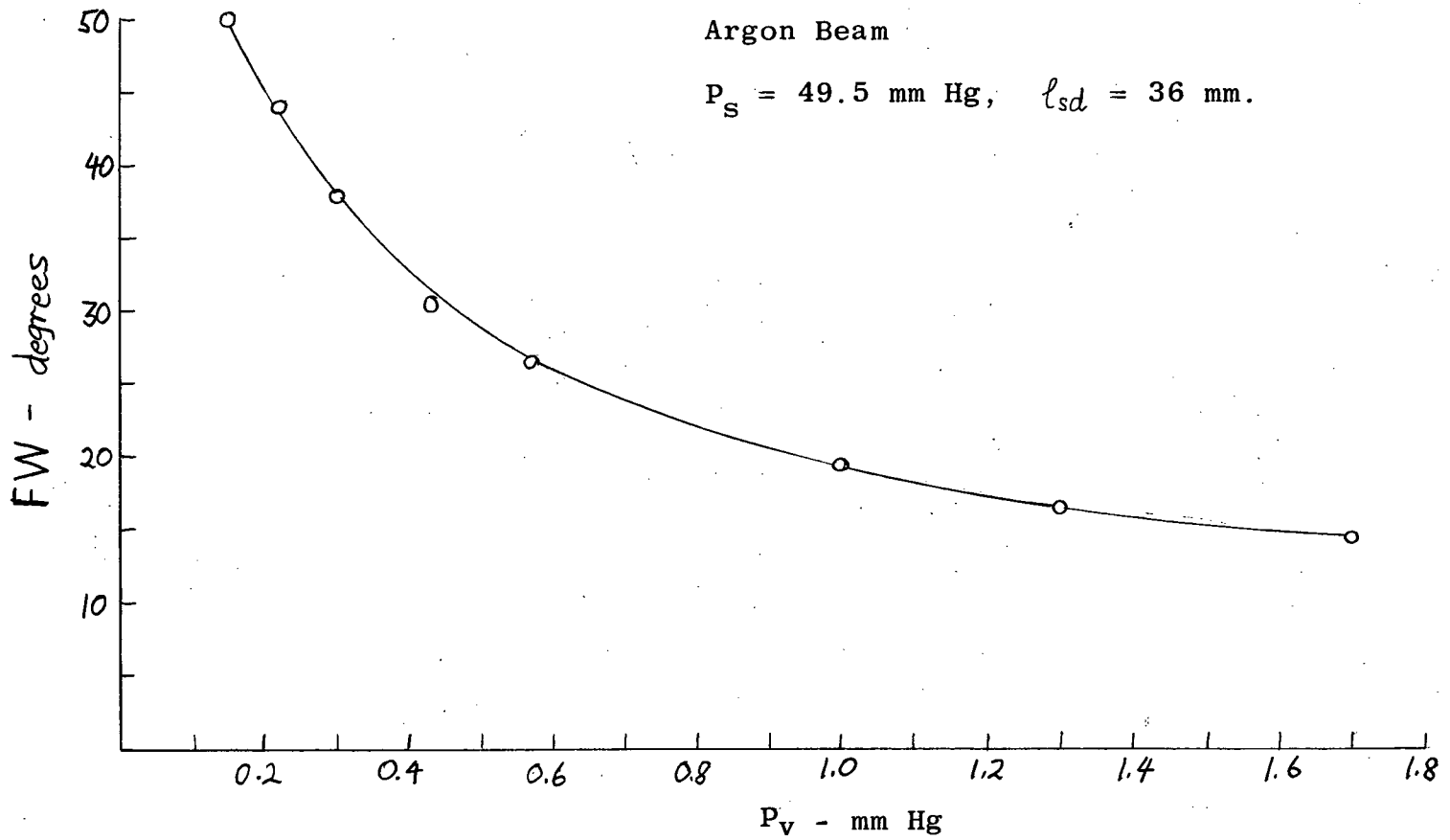

FIGURE 21. Effect of the Residual Gas Pressure on the Spatial Distribution of the Directional Kinetic Energy of a Nozzle Beam.

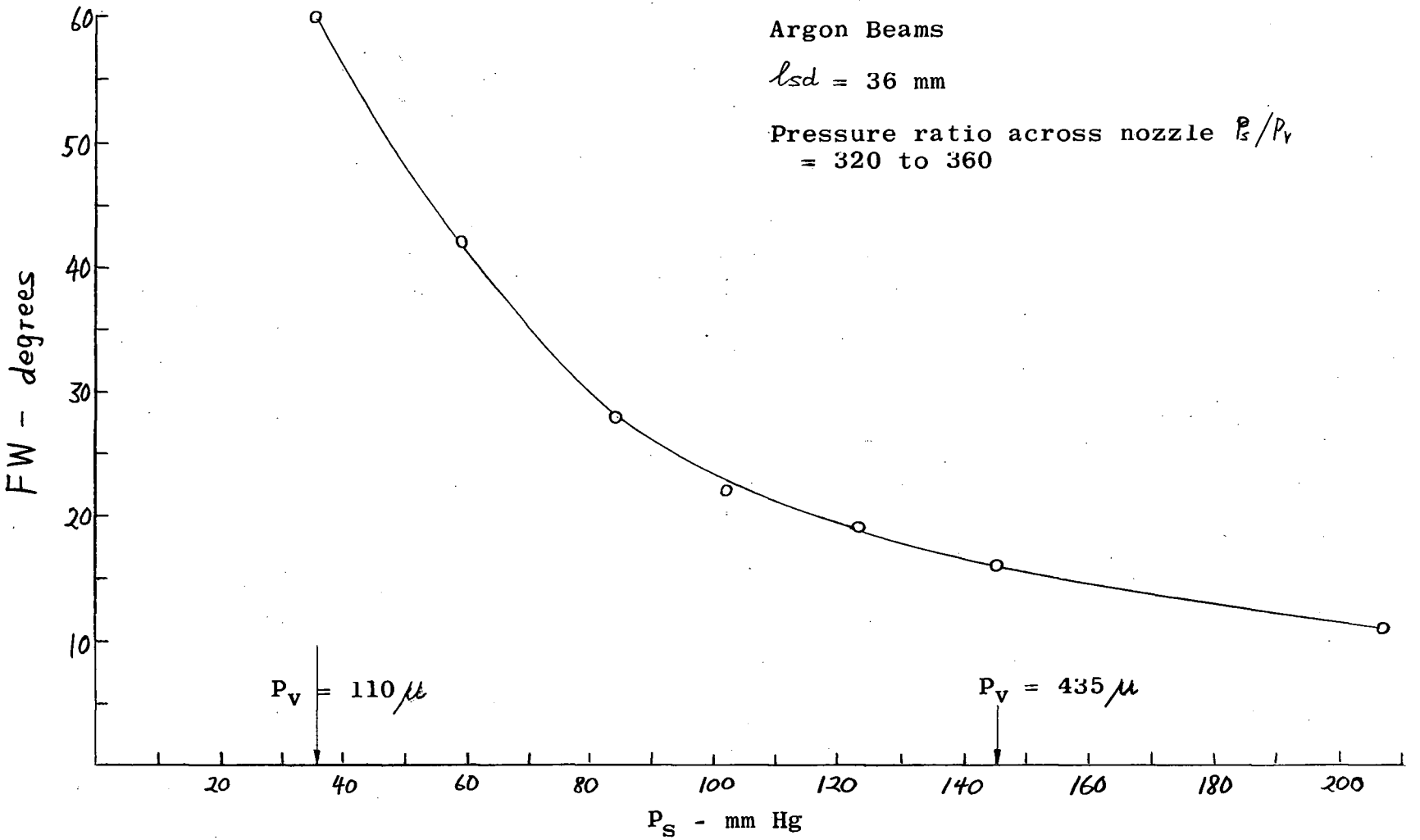

FIGURE 22. Effect of the Source and Residual Gas Pressures on the Spatial Distribution of the Directed Kinetic Energy of Nozzle Beams.

FIGURE 23. Spatial Distributions of the Directed Kinetic Energy of Two Nozzle Beams

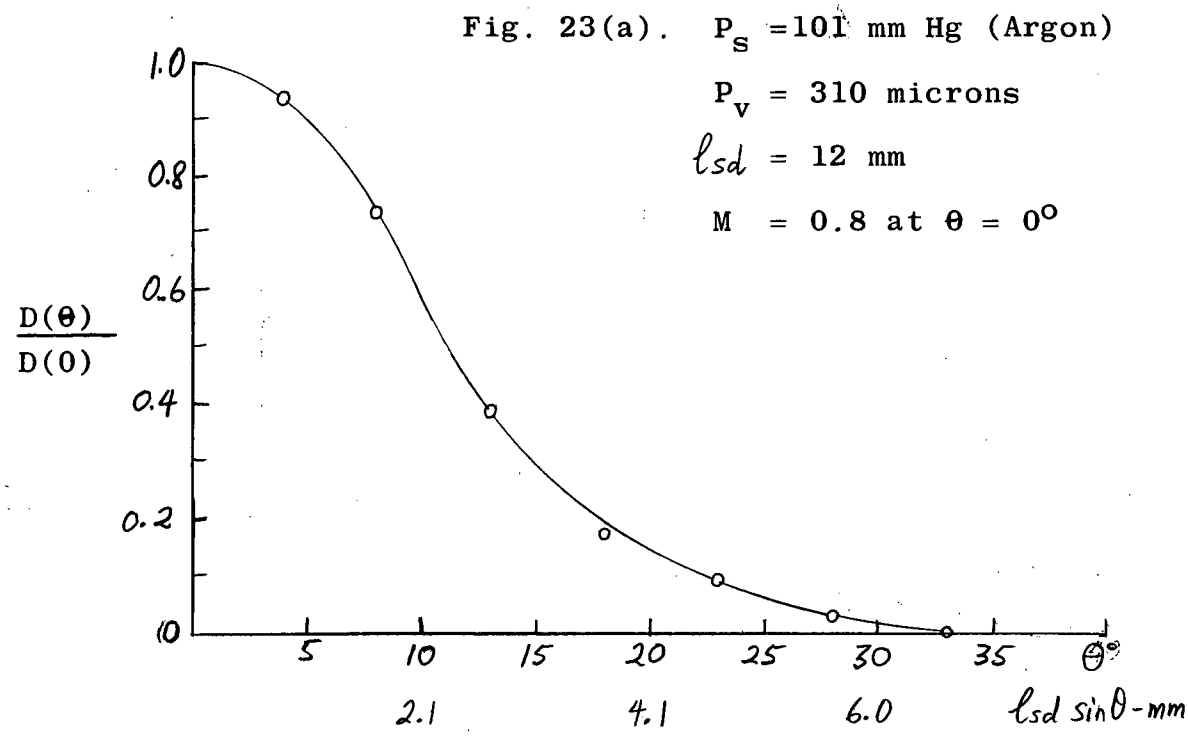

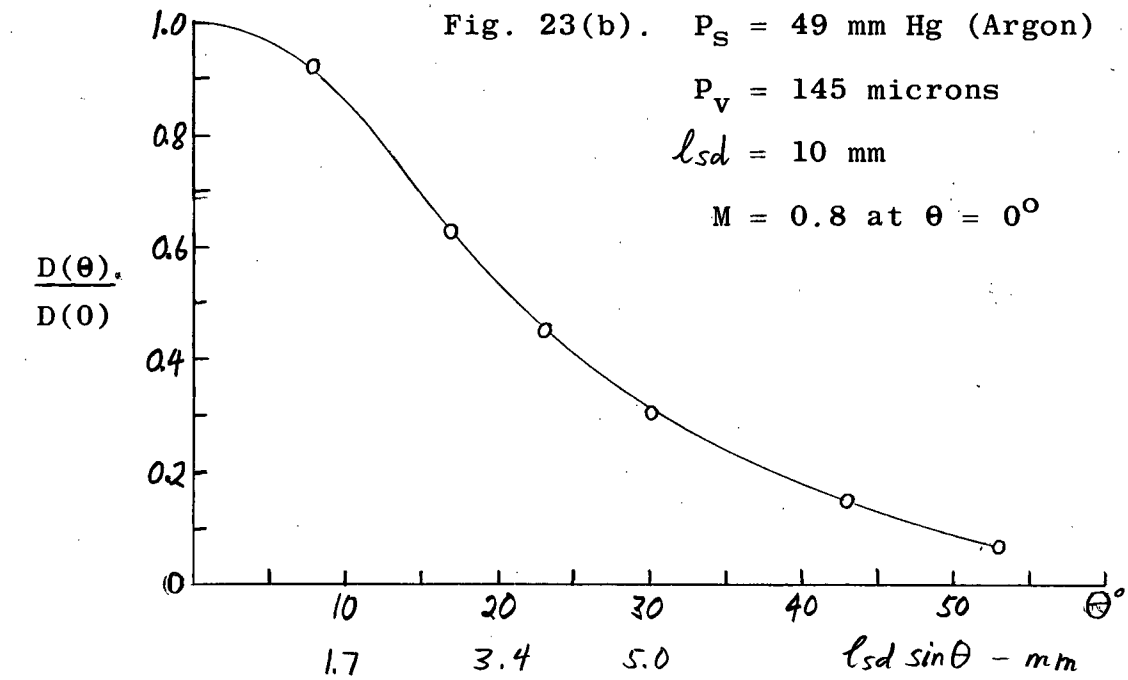

D. Conclusions

Consider a line perpendicular to the nozzle axis at point A (Figure 20). If one assumes that the flow velocity v of the beam is constant in magnitude at points along this line, then measurements such as those in Figure 23 give the relative mass density ρ and particle density $n = \frac{\rho}{m}$ of the beam at these points. Although one could then derive a beam intensity nv from this, there is no indication whatever of the direction of flow of the beam at *any* point. Thus unless a direction-finding Pitot tube is used (Liepmann and Roshko, 1957), measurements such as these can give no information about the beam directivity which might be useful in choosing optimum values of skimmer diameter and nozzle-skimmer distance. At any rate, the assumption mentioned above must be justified.

The best method of obtaining maximum beam intensity beyond the skimmer, for given pressure conditions, is probably the empirical one of observing the intensity as the nozzle-skimmer distance is varied.

APPENDIX A

THEORETICAL ANALYSIS OF THE DIFFERENTIAL PIRANI DETECTOR

Calculations similar to some of the following have been carried out by Knauer and Stern, 1929, Ellett and Zabel, 1931, and Ramsey, 1956. In the following analysis, the residual gas molecules in the beam gauge are not considered, since their effect is exactly cancelled by the effect of the residual gas molecules in the compensating gauge.

M.K.S. units are used in the numerical work.

1. Equilibrium Pressure and Time Constant

Suppose the detector entrance channel, K_1, is aligned parallel to the flow direction of an incident molecular beam (Figure 1). Then the number of molecules/sec entering the beam cavity, C_1, is: $I\ A_d$, and the number of molecules/sec leaving is: $\dfrac{1/4\ n_d\ \overline{v_d}\ A_d}{K}$

where I = incident beam intensity,

A_d = cross-sectional area of K_1,

n_d = no. of molecules per unit volume in C_1,

$\overline{v_d}$ = average velocity of the molecules in C_1,

K = kappa-factor of K_1 (page 5).

Now $n_d = P_d / (k\ T_d)$ and $\overline{v_d} = \sqrt{\dfrac{8kT_d}{\pi\ m}}$

where P_d = pressure in C_1 due to the beam molecules,

T_d = temperature of the detector block,

k = Boltzmann's Molecular Gas Constant,

m = mass of a beam molecule.

$$\therefore \quad \frac{1/4\, n_d \bar{v}_d A_d}{K} = \frac{P_d A_d}{K\sqrt{2\pi m k T_d}}$$

The rate of increase of the number of molecules in C_1 is

$$\frac{dN}{dt} = \frac{V_d}{kT_d}\frac{dP_d}{dt} = I A_d - \frac{P_d A_d}{K\sqrt{2\pi m k T_d}}$$

where V_d = volume of C_1.

The solution of this equation is

$$P_d = K I \sqrt{2\pi m k T_d}\left\{1 - \exp\left(-\frac{A_d}{K V_d}\sqrt{\frac{kT_d}{2\pi m}}\, t\right)\right\} \qquad \text{(Eq.A-1)}$$

Thus the time constant for filling and emptying C_1 is

$$\tau = \frac{K V_d}{A_d}\sqrt{\frac{2\pi m}{k T_d}} \qquad \text{(Eq.A-2)}$$

In the present case, V_d = 1.3 cc, $A_d = \pi/4 \times (0.80)^2$ mm^2, K = 28, and m = 5.01×10^{-27} Kg for Helium-3.

If $T_d = 293^{\circ}$K,

$$\tau = \frac{28 \times 1.3 \times 10^{-6}}{\pi/4 \times (0.80)^2 \times 10^{-6}}\sqrt{\frac{2\pi \times 5.01 \times 10^{-27}}{1.38 \times 10^{-23} \times 293}}$$

$$= \underline{0.20\text{sec}}.$$

If $T_d = 77^{\circ}$K, $\tau = 0.20 \times \sqrt{\frac{293}{77}} = \underline{0.39\ \text{sec}}$.

From Eq. A-1, the equilibrium pressure in C_1 is

$$P_d = K I \sqrt{2\pi m k T_d} \qquad \text{(Eq.A-3)}$$

Let K = 1 and I = 10^{13} atoms/sec/cm^2 of Helium-3.

If $T_d = 293^oK$,

$$P_d = 10^{17} \times \sqrt{2\pi \times 5.01 \times 10^{-27} \times 1.38 \times 10^{-23} \times 293} \left(\frac{1}{133}\right)$$

$$= \underline{8.5 \times 10^{-9} \text{ mm Hg.}}$$

If $T_d = 77^oK$, $P_d = 8.5 \times 10^{-9} \sqrt{\frac{77}{293}} = \underline{4.4 \times 10^{-9} \text{ mm Hg.}}$

2. Dependence of the Filament Temperature on Changes in Cavity Pressure.

The filaments lose heat mainly by radiation and gas conduction (page 9).

The rate of heat loss by radiation is

$$H_1 = \epsilon \sigma \left(T_f^4 - T_d^4\right) S \qquad \text{(Eq. A-4)}$$

where ϵ = emissivity of the W-2 filaments = 0.4,

σ = radiation constant = 5.67×10^{-8} M.K.S. units,

S = surface area of one W-2 filament = 0.0377 in^2,

T_f = filament temperature.

The rate of heat loss by gas conduction is

H_2 = no. molecules/sec striking unit area of filament x S x energy given each reflected molecule

$$= 1/4\, n_d\, \overline{v_d} \times S \times \frac{C_v}{N_o} \alpha (T_f - T_d)$$

$$= \frac{P_d}{\sqrt{2\pi\, m\, k\, T_d}} \frac{C_v}{N_o} \alpha S (T_f - T_d) \qquad \text{(Eq. A-5)}$$

where C_v = specific heat per mole at constant volume, which for He^3 is 1.25×10^4 M.K.S. units,

N_o = Avogadro's Number = 6.03×10^{26} M.K.S. units.

α = accomodation coefficient for He^3 on the fil-

ament surface; i.e., the ratio of the average energy actually given up by the filament to molecules which fall on the surface and are reflected, to the average energy which would be imparted if the molecules took up the filament temperature. For He^3, α is taken as 0.4, the average value for He^4 on a gas-contaminated tunsten surface at 300-500°K (White, 1959).

$$\text{Let } \beta = \frac{C_v \alpha}{N_o \sqrt{2\pi m k T_d}}$$

If E is the electrical power supplied to each filament,

$$E = H_1 + H_2$$

$$= \epsilon \sigma \left(T_f^4 - T_d^4\right) S + \beta P_d S (T_f - T_d)$$

We assume that the power supplied to the filaments is constant, since the bridge current may readily be made constant, and the filament resistance changes are small.

$$\frac{dE}{dP_d} = 0$$

$$4 \epsilon \sigma S T_f^3 \frac{dT_f}{dP_d} + \beta S (T_f - T_d) + \beta S P_d \frac{dT_f}{dP_d} = 0$$

$$\frac{dT_f}{dP_d} = \frac{-\beta (T_f - T_d)}{4 \epsilon \sigma T_f^3 + \beta P_d} \qquad \text{(Eq. A-6)}$$

With $T_d = 293°K$, previous Pirani detectors have operated at $T_f \approx 400°K$. Using these temperatures,

$$4 \epsilon \sigma T_f^3 = 4 \times 0.4 \times 5.67 \times 10^{-8} \times (400)^3$$

$$= 5.8 \text{ in M.K.S. units.}$$

Also, $$\beta = \frac{1.25 \times 10^{4} \times 0.4}{6.03 \times 10^{26} \times \sqrt{2 \times \pi \times 5.01 \times 10^{-27} \times 1.38 \times 10^{-23} \times 293}}$$

$$= 0.73 \quad \text{in MKS units.}$$

Eq. A-5 is valid only when there are no collisions between gas molecules in C_1; i.e., the mean-free-path in C_1 must be at least four times the maximum dimension of C_1. If the latter is 1.5 cm, then for this analysis to be valid, P_d must be less than 2 microns for He^3 at 293°K.

Thus $\beta P_d < 0.73 \times 2 \times 10^{-3} \times 133 = 0.19$. MKS

Hence $4 \epsilon \sigma T_f^3 >> \beta \times P_d$, and Eq. A-6 becomes

$$\frac{dT_f}{dP_d} \doteq \frac{-\beta (T_f - T_d)}{4 \epsilon \sigma T_f^3} \qquad \text{(Eq. A-7)}$$

Similar considerations for $T_d = 77°K$ indicated that Eq. A-7 is valid for $P_d < 0.5$ micron.

3. <u>The Detector Output Signal as a Function of Pressure</u>

$$H_1 = \epsilon \sigma \left(T_f^4 - T_d^4\right) S$$

$$= 0.4 \times 5.67 \times 10^{-8} \times \left[(400)^4 - (293)^4\right] S$$

$$= 412 \, S$$

$$H_2 = \beta P_d (T_f - T_d) S < .19 \times 107 \, S = 20 \, S << H_1$$

Thus practically all the power supplied to the filaments is dissipated by radiation. If I_f is the filament current and R_f the filament resistance,

$$I_f^2 R_f = \epsilon\sigma\left(T_f^4 - T_d^4\right) S$$

$$I_f = \sqrt{\frac{\epsilon\sigma\left(T_f^4 - T_d^4\right) S}{R_f}} \qquad \text{(Eq. A-8)}$$

When $P_d = 0$, the four filaments, if identical, each have resistance R_f. When a molecular beam is directed into C_1, $P_d > 0$ and each of the two filaments in C_1, R_1 and R_2, (Figure 2), decreases its resistance by

$$dR = R_f \, c \, dT_f$$

where c = temperature coefficient of resistance of the W-2 filament = 0.005,

and dT_f is given by Eq. A-7.

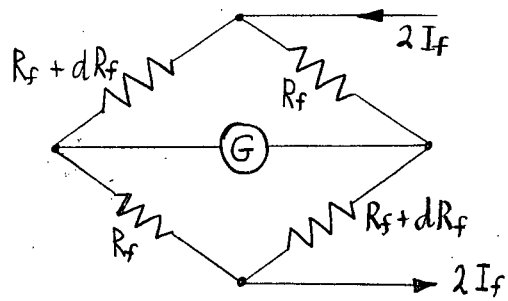

In the present case the bridge galvanometer G has resistance much greater than R_f, and so draws negligible current. If the bridge is supplied with a constant-current source, the detector output signal, in volts, is

$$dV = I_f (R_f + dR) - I_f R_f$$

$$= I_f \, dR = I_f R_f \, c \, dT_f \qquad \text{(Eq. A-9)}$$

Substituting Eqs. A-7 and A-8 in Eq. A-9, and dropping the minus sign,

$$dV = \sqrt{\frac{\epsilon\sigma\left(T_f^4 - T_d^4\right) S}{R_f}}\; R_f\, c\, \frac{\beta\,(T_f - T_d)}{4\,\epsilon\,\sigma\,T_f^3}\, dP_d$$

$$= \frac{(T_f - T_d)}{T_f^3} \sqrt{\left(T_f^4 - T_d^4\right) R_f}\; \sqrt{\frac{S}{\sigma\epsilon}}\; \frac{c\beta}{4}\, dP_d$$

(Eq. A-10)

The voltage output increases with increasing T_f. However, as discussed on page 11, the maximum T_f to consider is $T_f = 560^{\circ}K$. Substituting this value for T_f, then at $T_d = 293^{\circ}K$ and $K = 1$, a He^3 beam of intensity 10^{13} atoms/sec/cm^2 will produce a signal

$$dV = \frac{(560 - 293)}{(560)^3} \sqrt{(560)^4 - (293)^4}\; \times 92$$

$$\times \sqrt{\frac{0.0377 \times 6.45 \times 10^{-4}}{5.67 \times 10^{-8} \times 0.4}}\; \times \frac{0.005 \times 0.73}{4}$$

$$\times \quad 8.5 \times 10^{-9} \quad \times \quad 133$$

$$= \underline{0.15 \text{ microvolt}}.$$

At $T_d = 77^{\circ}K$ and $K = 1$, the same beam intensity will produce a signal of dV = <u>0.28 microvolt</u>, as shown by a calculation similar to the above.

APPENDIX B

TRANSISTORIZED IONIZATION GAUGE CONTROL CIRCUIT

1. Introduction

Several control units were required for the many ionization gauges which had been installed in vacuum systems in this laboratory. Since commercially available units cost at least $450 (U.S.) each, it was decided to attempt to construct suitable control circuits at considerably less expense. Eleven control units were built at a cost of about $110 each for components, electrical and mechanical. The 710 - cu.in. chassis can be rackmounted (19" rack) and weighs about 16 lb. The prototype unit has operated for more than one year without failure of any kind, while the others have operated successfully for many months.

2. Operation of the Hot-cathode Ionization Gauge

Detailed descriptions of ionization gauges and the requirements of their electric controls can be found in several books on vacuum technique (e.g., Pirani and Yarwood, 1961; Dushman and Lafferty, 1962).

Basically, the Bayard-Alpert ion gauge (Bayard and Alpert, 1950) consists of three electrodes (Figure 24). The directly-heated filament F emits electrons which are accelerated toward the positive grid G. The positive ions produced by collision of these electrons with the residual gas mole-

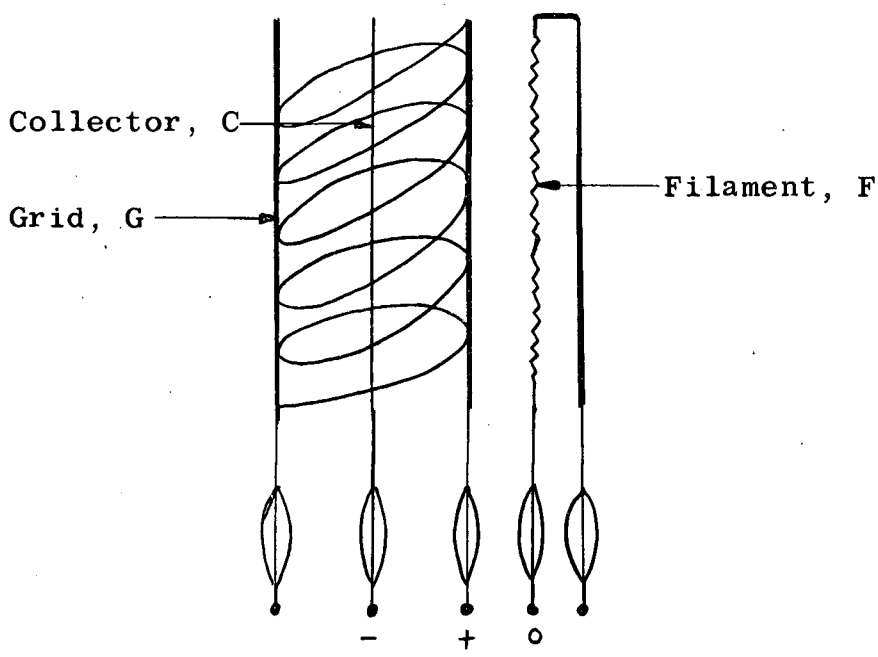

$V_G - V_F = +150$ to $+200$ Volts

$V_C - V_F = -5$ to -30 Volts.

FIGURE 24. Schematic Diagram of the Bayard-Alpert Ionization Gauge.

cules are attracted to the negative collector C. The positive ion current is directly proportional to the gas pressure P_v, if $P_v < 10^{-4}$ mm Hg. If $P_v > 10^{-4}$ mm Hg, the ion current may be a non-linear function of P_v, and above 1 micron discharges may occur.

The ion gauges in this laboratory have a sensitivity for dry air of 100 μA/micron when the grid current is 5.0 mA, provided the grid is maintained at +180-200 V and the collector at about -25 V with respect to the filament.

3. General Description of the New Control Circuit.

A transistorized circuit was designed specifically to control the ion gauges of this lab., although most commercial ion gauges could be controlled with this unit with minor modifications, if any.

In this circuit the filament is maintained at about 28 V with respect to ground, while the grid is supplied with a regulated 210 V. To produce a constant grid (or emission) current, I_g, a transistor-controlled saturable reactor is used to regulate filament current in the range 1.6 to 6.0 A, with no significant heat dissipated in the control box.

The ion current, I_c, to the collector, maintained at -23 to -28 V with respect to the filament, is measured with a simple current-feedback transistorized dc amplifier, which is useful down to I_c = 1 nA. The pressure range is divided into four decades, the most sensitive being 10^{-6} mm Hg F.S.D.,

corresponding to 100 nA I_c (dry air) when I_g = 5.0 mA.

A safety circuit shuts off the filament current when the pressure rises to some preset value, thus preventing damage to the filament and to the sensitive meter of the I_c amplifier.

4. Detailed Description of the New Control Circuit.

The complete circuit diagram is shown in Figure 25. T10 and T11 with the saturable reactor and filament transformer comprise a grid-current-regulated filament supply. I_g may be set to any value between about 2 and 20 mA by potentiometer R4. I_g is maintained at this value by comparing the voltage drop produced by I_g across R4 and R5 with the zener-regulated 28 V applied to the base of the comparator T10 (D. Skaperdas and H. Tomaschke, 1961; Winkler, 1963). If, for example, I_g decreases, the conduction of T10 drops, thereby increasing the conduction in T11 and raising the current through the dc coil of the saturable reactor. The core of the saturable reactor is then driven further into saturation so that its ac reactance decreases and a larger voltage is applied to the filament transformer, thereby increasing I_g.

The filaments used have been both 5- and 10- mil tungsten filaments which required currents in the range 1.6 to 6.0 A at voltages of 3.0 to 6.5 V to produce I_g from 2 to 20 mA. Once set, I_g remains constant as the pressure varies

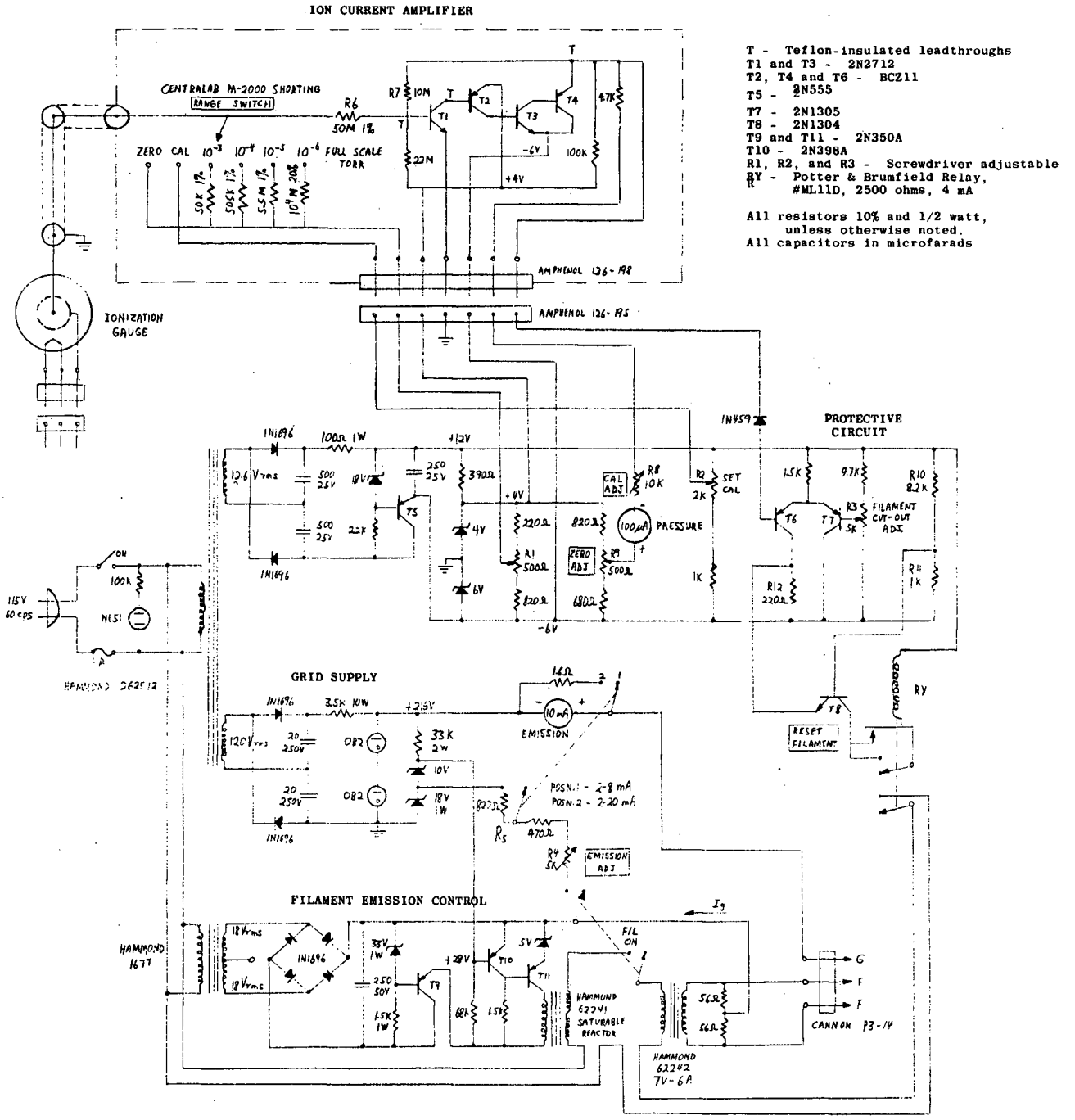

FIGURE 25. Transistorized Ionization Gauge Control Circuit.

over the range of 1 x 10^{-7} to 1 x 10^{-4} mm Hg, but increases by 3% between 1 x 10^{-4} and 5 x 10^{-4} mm Hg.

The GE 2n2712 and Philips BCZ11 in the I_c amplifier are inexpensive transistors with leakage currents of less than 1 nA and current gains of more than ten at a collector current of 1 μA. The epoxy casing of the 2N2712 must be shielded from light (e.g., by wrapping the casing in black tape or coating with black paint) to obtain the low leakage currents quoted.

In each range-switch position, the portion of I_c which passes through R6 into the virtual earth input of the amplifier is 0-100 nA. Variation in the base voltage of T1 for these signal currents are less than 20 mV above the quiescent value of about 350 mV. A constant proportion of the input current flows through the feedback resistor R7, producing an output voltage change of up to -0.95 V.

The centertap voltage of R1 is set to the base voltage of T1 by first turning off the filament, then adjusting R1 so that the reading on the 10^{-3} mm Hg scale is the same as the reading on the 10^{-6} mm Hg scale, which is unaffected by R1. The large resistance R6 prevents significant current flowing between R1 and T1 due to changes in the base-emitter voltage of T1 with moderate temperature variations. The voltage drop across R6 due to the ion current causes the collector voltage to vary between -28 and -23 V with respect to the filament, but with the gauges of this lab. this

results in an error of less than 2%. For a gauge whose sensitivity is I_o μA at 10^{-4} mm Hg, the centertap voltage of R2 (set Cal) is set to 0.5 x I_o V above the base voltage of T1. After setting the zero by adjusting R9, the amplifier is then calibrated on the CAL position by adjusting R8 until the meter reads 100 μA.

To eliminate the problem of leakage currents in the chassis, the I_c amplifier is contained in a small Aluminum box with the input resistors mounted on the steatite range switch. Several teflon-insulated standoffs are used and the collector lead is well-shielded.

After initial warmup of 15 to 30 minutes, the zero drift of the I_c amplifier in 24 hr is less than 3% of full scale, while variation in I_g is less than 1%. For a line-voltage variation of 100 to 130 Vac, the I_c amplifier zero changes by 3% of full scale, while I_g changes by less than 1%.

The filament power is automatically shut off by the protective relay RY when the I_c amplifier output exceeds the value set by potentiometer R3. The range of values allowed for are between the zero of the pressure meter and more than five times full scale. Because T6 is normally biased off, T8 conducts 7 mA, a value determined by the bias resistors R10 and R11 and the emitter load R12. When the base voltage of T6 falls below that of T7, T6 is turned on, T7 and T8 are turned off, and the relay contacts open. The 1N459 diode prevents the leakage current of T6 from interfering with the

I_c amplifier.

The power transistors, T5, T9 and T11, which dissipate less than one watt each, are mounted on simple heat sinks. The total power consumption is less than 100 W, of which about 10 W are dissipated in the control box.

5. Deficiencies of the Circuit

With some filaments in certain vacuum systems, I_g tends to oscillate for pressures greater than 5×10^{-5} mm Hg, presumably because the control circuit cannot compensate for the time lag of filament emission, which is especially troublesome when there is some contaminant on the filament surface. This problem has often plagued hot-cathode control circuits (Leck, 1957).

A more sensitive ion current amplifier is needed in order to extend accurate pressure measurements below 10^{-7} mm Hg.

For operation at pressures below 10^{-7} mm Hg, there should be provision for degassing the gauge before use, preferably by direct heating of the grid (Pirani and Yarwood, 1961). At present only the filament surface can be degassed, by increasing the filament current.

APPENDIX C

MEASUREMENT OF FLOW RATE THROUGH NOZZLES

Figure 26 shows the apparatus used to measure flow rates through nozzles. V_3 is closed, while V_1 and V_2 are initially open, thus maintaining a constant gas flow to the oven and nozzle. The manometer pressure is initially $P_a + h_1$, where P_a is the atmospheric pressure. V_2 is then closed, so that after time t the pressure in the measuring system is reduced to $P_a + h_2$.

Let V_o be the volume of the measuring system when the pressure is P_a and suppose each arm of the manometer has cross-sectional area A. Then the gas flow per unit time (throughput) through the nozzle, in units of pressure X volume, is

$$G = \frac{1}{t}\left\{(P_a + h_1)\left(V_o + \tfrac{1}{2}h_1 A\right) - (P_a + h_2)\left(V_o + \tfrac{1}{2}Ah_2\right)\right\}$$

$$= \frac{P_a \Delta V}{t}\left\{\frac{1}{2} + \frac{\Delta h}{P_a}\left(\frac{V_o}{\Delta V} + \frac{h_1 + h_2}{2\Delta h}\right)\right\} \qquad \text{(Eq. C-1)}$$

where $\Delta h = h_1 - h_2$ and $\Delta V = A\,\Delta h$

If $\frac{V_o}{\Delta V} >> \frac{h_1 + h_2}{2\Delta h}$ and $\frac{V_o}{\Delta V}\frac{\Delta h}{P_a} >> \frac{1}{2}$

then $G \approx \frac{\Delta h\, V_o}{t}$ $\frac{\text{mmHg - cc}}{\text{sec}}$ or $\frac{\text{micron-liters}}{\text{sec}}$

(Eq. C-2)

V_o was measured to 1% accuracy by filling the system to a pressure of about 2 atmospheres with argon, and then expanding this gas through V_3 into an evacuated container of

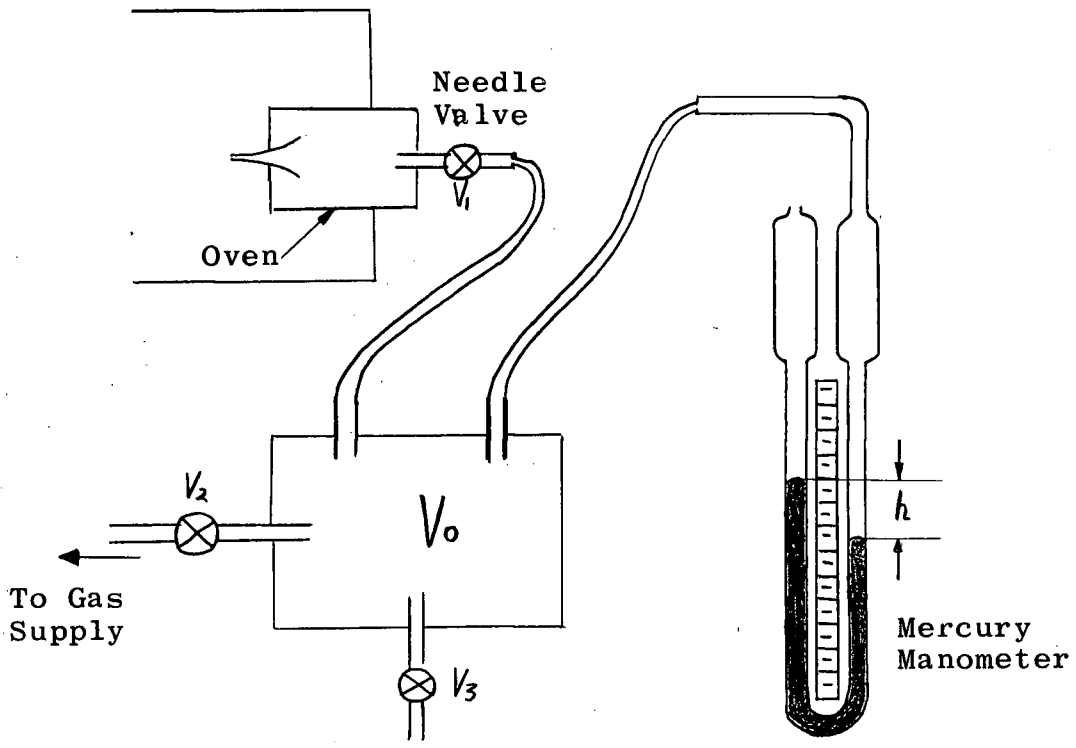

FIGURE 26. Apparatus for Measuring Rate of Gas Flow through Nozzles.

exactly known volume. The value of V_o thus found was 538 cc. The system was leaktested by pumping through V_2 and observing readings of a thermocouple gauge attached at V_3.

By working out a few cases in the range of interest, it appeared that Eq. C-2 gave values about 2% smaller than the accurate values calculated from Eq. C-1, so all measured flow rates obtained from Eq. C-2 were increased by 2%. $\underline{t}$ was always chosen long enough to enable Δh to be measured with 1 to 5% accuracy; during this time interval, P_s decreased by 1-2%.

BIBLIOGRAPHY

Axen, D., Klinger, W. and Warren, J.B. (1963), Progress in Fast Neutron Physics, Rice University Semicentennial Publications.

Bayard, R.T., and Alpert, D. (1950), Rev. Sci. Instr., 21, 571.

Becker, E.W., and Bier, K. (1954), Z. Naturforsch 9a, 975.

Clausing, P. (1930), Z. f. Physik 66, 471.

Clausing, P. (1932), Ann. d. Physik 12, 961.

Dayton, B.B. (1956), Vacuum Symposium Transactions, 1956, 5.

Deckers, J. and Fenn, J.B. (1963), Rev. Sci. Instr., 34, 96.

Devienne (1960), Proceedings of the First International Symposium on Rarefied Gas Dynamics, Pergamon Press.

Dushman, S., and Lafferty, J.M. (1962), Scientific Foundations of Vacuum Technique, John Wiley & Sons, Inc., New York.

Ellett, A. (1931), Phys. Rev. (2), 37, 1699.

Ellett, A., and Zabel, R.M. (1931), Phys. Rev. 37, 1112.

Giordmaine, J.A., and Wang, T.C. (1959), J. Appl. Phys. 31, 463.

Gunther, K.G. (1957), Zs. angew. Phys. 9, 550.

Helmer, J.C., Jacobus, F.B. and Sturrock, W.W. (1960), J. Appl. Phys. 31, 458.

Hurlbut, F.C. (1958), Paper UA-5, American Physical Society.

Ivanov, B.S. and Troitskii, V.S. (1963), Soviet Physics - Technical Physics 8, 365.

King, J.G. and Zacharias, J.R. (1956), Advances in Electronics and Electron Physics 8, 1.

Knauer, F. and Stern, O. (1929), Zeits. f. Physik 53, 766.

Knudsen, M. (1909), Ann. Physik 28, 76 and 999.

Kolsky, H.G., Phipps, Jr., T.E., Ramsey, N.F. and Silsbee, H.B. (1952), Phys. Rev. 87, 395.

Korsunsky, M., and Vekshinsky, S. (1945), J. Phys., U.S.S.R., 9, 399.

Leck, J.H. (1957), Pressure Measurement in Vacuum Systems, Chapman and Hall, London.

Liepmann, H.W., and Roshko, A. (1957), Elements of Gasdynamics, John Wiley & Sons, Inc., London.

Mayer, H. (1928), Zeits. f. Physik, 52, 235.

Mayer, H. (1929), Zeits. f. Physik, 58, 373.

Minten, A., and Osberghaus, O. (1958), Zeits. f. Physik, 150, 74.

Naumov, A.I. (1963), Soviet Physics - Technical Physics 8, 88.

Pirani, M., and Yarwood, J. (1961), Principles of Vacuum Engineering, Reinhold Publishing Corp., New York.

Ramsey, N.F. (1956), Molecular Beams, Oxford University Press.

Shapiro, A.H. (1953), The Dynamics and Thermodynamics of Compressible Fluid Flow, Vol. 1, Ronald Press, New York.

Skaperdas, D. and Tomaschke, H. (1961), Rev. Sci. Instr. 32, 1961.

Smith, K.F. (1955), Molecular Beams, Methuen & Co. Ltd., London.

Troitskii, V.S. (1962), Soviet Physics-Technical Physics, 7, 353.

Vermette, C.W. (1964), M.A.Sc. Thesis, U.B.C.

White, G.K. (1959), Experimental Techniques in Low Temperature Physics, Clarendon Press.

Winkler, H. (1963), Rev. Sci. Instr. 34, 295.

Yarwood, J. (1956), High Vacuum Technique, Chapman and Hall, London.